

## Primer



# Light-based vat-polymerization bioprinting

Riccardo Levato<sup>1,2</sup>✉, Oksana Dudaryeva<sup>2</sup>, Carlos Ezio Garciamendez-Mijares<sup>3</sup>, Bruce E. Kirkpatrick<sup>4,5,6</sup>, Riccardo Rizzo<sup>7,8,9</sup>, Jacob Schimelman<sup>10</sup>, Kristi S. Anseth<sup>4,5</sup>, Shaochen Chen<sup>10</sup>, Marcy Zenobi-Wong<sup>7</sup> & Yu Shrike Zhang<sup>10</sup>✉

## Abstract

Light-based vat-polymerization bioprinting enables computer-aided patterning of 3D cell-laden structures in a point-by-point, layer-by-layer or volumetric manner, using vat (vats) filled with photoactivatable bioresin (bioresins). This collection of technologies – divided by their modes of operation into stereolithography, digital light processing and volumetric additive manufacturing – has been extensively developed over the past few decades, leading to broad applications in biomedicine. In this Primer, we illustrate the methodology of light-based vat-polymerization 3D bioprinting from the perspectives of hardware, software and bioresin selections. We follow with discussions on methodological variations of these technologies, including their latest advancements, as well as elaborating on key assessments utilized towards ensuring qualities of the bioprinting procedures and products. We conclude by providing insights into future directions of light-based vat-polymerization methods.

## Sections

Introduction

Experimentation

Results

Applications

Reproducibility and data deposition

Limitations and optimizations

Outlook

<sup>1</sup>Department of Clinical Sciences, Faculty of Veterinary Medicine, Utrecht University, Utrecht, Netherlands.

<sup>2</sup>Department of Orthopedics, University Medical Center Utrecht, Utrecht, Netherlands. <sup>3</sup>Division of Engineering in Medicine, Brigham and Women's Hospital, Department of Medicine, Harvard Medical School, Cambridge, MA, USA. <sup>4</sup>Department of Chemical and Biological Engineering, University of Colorado Boulder, Boulder, CO, USA. <sup>5</sup>BioFrontiers Institute, University of Colorado Boulder, Boulder, CO, USA. <sup>6</sup>Medical Scientist Training Program, University of Colorado Anschutz Medical Campus, Aurora, CO, USA. <sup>7</sup>Department of Health Sciences and Technology, ETH Zürich, Zürich, Switzerland. <sup>8</sup>Wyss Institute for Biologically Inspired Engineering, Harvard University, Boston, MA, USA. <sup>9</sup>Harvard John A. Paulson School of Engineering and Applied Sciences, Harvard University, Boston, MA, USA. <sup>10</sup>Department of NanoEngineering, University of California San Diego, La Jolla, CA, USA. ✉e-mail: [r.levato@uu.nl](mailto:r.levato@uu.nl); [yszhang@research.bwh.harvard.edu](mailto:yszhang@research.bwh.harvard.edu)

## Introduction

Three-dimensional bioprinting utilizes computer-aided processes to spatially pattern cells and/or auxiliary biomaterials to enable creation of functional bioengineered structures for various applications in biomedicine<sup>1–6</sup>. Light-based vat polymerization was the first 3D printing method developed back in 1986 in the form of stereolithography<sup>7</sup>. Nevertheless, its biomedical utility<sup>8,9</sup> and, in particular, expansion into bioprinting – with cell loading into photopolymerizable hydrogels during the printing procedure – was not demonstrated until almost two decades later<sup>10</sup>.

Over the years, light-based vat-polymerization bioprinting has witnessed notable advancements across all aspects, through hardware optimizations to biomaterial designs and downstream applications. According to modes of operation, this collection of technologies can be divided into those that pattern the bioresin point-by-point, layer-by-layer or directly volumetric; the specific modalities include lithographic techniques, such as stereolithography in its original implementation, utilizing single-photon lasers (SLA)<sup>11,12</sup>, multiphoton polymerization lithography (oftentimes adopting the two-photon mechanism, or TPL)<sup>12,13</sup>, digital light processing (DLP)<sup>11,12</sup> and volumetric bioprinting, also termed volumetric additive manufacturing (VAM)<sup>14–16</sup>. Despite these variations, a common feature of light-based vat-polymerization bioprinting methods is that they all rely on patterned light-dose distributions to initiate localized chemical reactions of photoactivatable bioresins. As the bioresins react in response to light, this results in the formation of desired structures in 2D and in 3D volumes. Although in most scenarios such chemical reactions are in the additive manner (for example, photocrosslinking), they can also be made subtractive such as with photodegradation<sup>17</sup>. Different modalities for shaping light in enabling layer-by-layer or volumetric development of these photoreactions exist, each spanning a defined range of resolution, speed of fabrication, required bioresin properties and therefore target applications.

This Primer intends to provide a thorough understanding of light-based vat-polymerization bioprinting, which forms a complementary toolset to another class of commonly used bioprinting methods relying on extrusion<sup>18</sup>. We present key considerations when selecting a light-based vat-polymerization bioprinting modality, relating to its hardware, software and bioresin designs. We further describe assessments that are essential to ensure robust bioprinting procedures, reporting requirements to maximize reproducibility, as well as limitations of current technologies and improvements that can be made to mitigate

these limitations. We finally conclude with future perspectives that involve discussions relating to integration of machine learning and translations.

## Experimentation

Light-based vat-polymerization bioprinting, compared with extrusion bioprinting<sup>18</sup>, generally provides improved controllability over structural complexity of the tissue constructs that can be produced at a faster fabrication rate and higher resolutions, although the specifications may depend on the specific modality adopted (Table 1). The use of patterned light requires precise calibration of light paths and associated bioprinting parameters to enable proper biofabrication of desired volumetric patterns. Such adjustments of light and operational parameters are all very specific to the vat-polymerization modality used, whether it is TPL (used throughout the Primer given its much broader usage than multiphoton polymerization lithography), SLA, DLP or VAM. It should be clarified that bioprinting by definition is a specific subset of 3D printing, in which 3D printing occurs in the presence of living cells<sup>1,19</sup>. The same distinction applies when referring to bioink and bioresin versus (biomaterial) ink and resin<sup>20</sup>. For the sake of consistency, we generally use the terminologies bioresin and bioprinting, although in certain specific descriptions resin and printing may also be used to indicate that cell-laden biofabrication has not yet been demonstrated.

## Bioprinter selection and setup

Vat-polymerization bioprinters can be generally classified by their modes of operations, depending on whether the light for photocrosslinking is projected in a single spot or as a plane and whether the patterning is performed linearly or rotationally. Point-by-point bioprinting relies on laser scanning given the single-spot nature of most laser systems. TPL is a typical bioprinter that utilizes the point-by-point scanning scheme, which builds volumetric structures by raster-scanning the two-photon laser spot across an area and repeating in the vertical direction for each layer to be produced<sup>13,21–23</sup> (Fig. 1a). A similar operation mode is adopted by the conventional SLA with SLA irradiation<sup>7,24,25</sup> (Fig. 1b). The raster-scanning approach provides efficient photoreactions owing to the larger power densities enabled by the laser lights; however, the inherent larger power densities result in a lower possible cell viability, and raster-scanning is usually a slow process especially when large build volumes are necessary. On the contrary, instead of raster-scanning, a single plane of light can be projected at once to enable simultaneous photocrosslinking of the desired pattern in that layer, followed by layer-by-layer construction leading to the 3D-bioprinted structure. A representative modality of layer-by-layer projection-based bioprinting is DLP bioprinting<sup>11,12,26</sup> (Fig. 1c). These DLP bioprinters use light-emitting diode arrays that directly emit patterned light<sup>27</sup> via liquid-crystal display screens that form digital masks in front of the light source to achieve patterned light<sup>28</sup> or digital micromirror array devices (DMDs) that reflect incident light to build patterns<sup>29–31</sup>.

Spatial light modulators such as DMDs are also core technologies in VAM. In this class of approaches, multiple planar light patterns are produced starting from either a laser light or a non-coherent light source and are subsequently projected across the entire volume of the vat<sup>32,33</sup>. The combination of these projections generates an anisotropic light-dose distribution within the vat, so that the cumulative light dose exceeds the polymerization threshold of the bioresin only in correspondence to the geometry of the object to be bioprinted. Currently,

**Table 1 | Key performance indicators for vat-polymerization bioprinting techniques**

Bioprinting technique	Minimum feature size	Bioresin viscosity	Modulus range	Time to build 1-cm <sup>3</sup> constructs
Extrusion	~100 µm <sup>227</sup>	0.005–100 Pas <sup>228</sup>	1–200 kPa <sup>229,230</sup>	Minutes–hours
TPL	2–8 µm <sup>154,158</sup>	>10 Pas	0.1–140 kPa <sup>140,231</sup>	Hours
SLA	5–10 µm <sup>232,233</sup>	0.25–10 Pas <sup>84</sup>	2–20 kPa <sup>143,234</sup>	Minutes–hours
DLP	10–50 µm <sup>30,111</sup>	0.25–10 Pas <sup>84</sup>	1–180 kPa <sup>110,111</sup>	Minutes
VAM	~40 µm <sup>33</sup>	>10 Pas <sup>37</sup>	0.4–25 kPa <sup>33,80</sup>	Seconds

The data refer to prints with cells but not acellular constructs. DLP, digital light processing; SLA, single-photon laser lithography; TPL, two-photon lithography; VAM, volumetric additive manufacturing.

# Primer

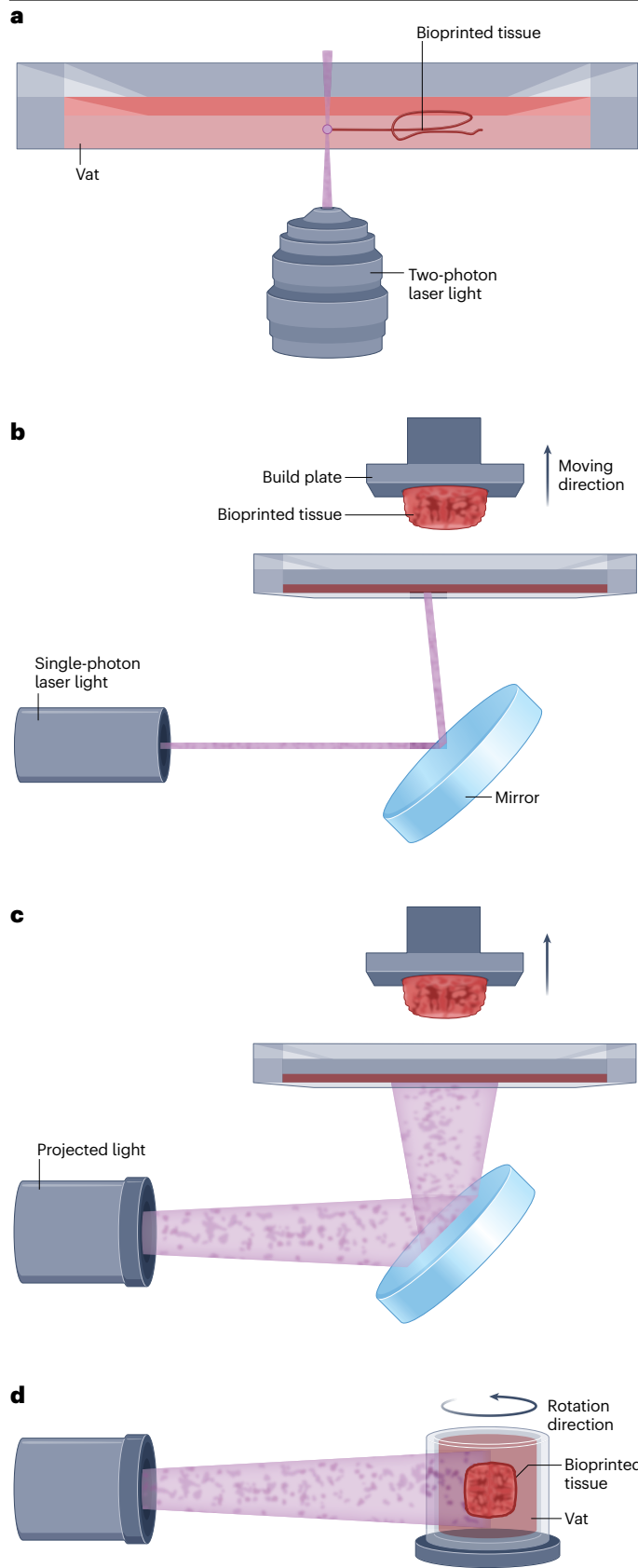


**Fig. 1 | Typical light-based vat-polymerization techniques.** **a**, Two-photon lithography that raster-scans two-photon lasers to polymerize or deconstruct a bioresin for 3D bioprinting. **b**, Single-photon stereolithography that raster-scans a single-photon laser for 3D bioprinting. **c**, Digital light processing that projects a series of light patterns to achieve layer-by-layer 3D bioprinting. The system shown is the bottom-up configuration. **d**, Tomographic bioprinting that projects a series of intensity-modulated light patterns to achieve rotational 3D bioprinting.

VAM is performed utilizing either a single light source projected onto a rotating vat (tomographic bioprinting)<sup>32–35</sup> (Fig. 1d) or multiple light sources delivered onto a static vat (holographic printing)<sup>15</sup> or systems in which a movable light sheet intersects orthogonally with DLP projections to trigger vat polymerization owing to uniquely designed photoinitiators (light-sheet 3D printing, also known as xolography)<sup>16</sup>.

Key considerations regarding the bioprinting modality to select include but are not limited to the resolution, the build volume, the speed and the cost. Laser-enabled vat-polymerization modalities such as TPL, SLA and VAM that contain high-quality laser systems are generally expensive in particular when multiphoton setups are needed, although resolutions are typically higher than when non-coherent light sources are used (from tens of nanometres for TPL to tens of micrometres for VAM). In comparison, DLP, as well as some VAM and SLA systems that use either non-laser light or low-power lasers, is more cost-efficient, despite the reduced resolutions (50–100- $\mu\text{m}$  range). Moreover, as the VAM process addresses the whole volume at once, manufacturing can occur at much high rates (<20 s to generate cubic-centimetre-sized constructs) than most other vat-polymerization strategies<sup>14</sup>.

## Software considerations

Software considerations for vat-polymerization bioprinting methods consist of three key components: voxels, which encode the desired input data to be bioprinted; a slicing algorithm, which converts the encoded data to a technique-specific output and synchronization, which brings together the projection system, motor and peripherals. Vat polymerization, in its simplest form, is the irradiation of light onto a photocurable bioresin; the light takes shape of either a specified point emitted from a laser (in the case of TPL and SLA), or a complete plane of image emitted from a projection device (in the case of DLP and VAM)<sup>6,36,37</sup>. Therefore, the main objectives are to produce, display and monitor these points or images in such a way that accurately reproduces the desired model. For the purpose of this section, software considerations are summarized without taking into account the influences exerted by the bioresin selection, bioresin kinematics and other bioresin-dependent factors. In addition, for computer-aided design software, the reader is referred to the Primer on extrusion bioprinting<sup>18</sup>.

**Voxels.** Voxels, also referred to as 3D pixels, and their applicability to 3D printing have been explored in great lengths owing to their potential to represent 3D volumes, standard tessellation language (STL) files, curves and equations and point clouds<sup>18,38,39</sup>. Voxelization converts input data, commonly STL files, to a conjunction of 3D pixels: a key concept that allows to factor in the limitations presented by the hardware into the software. As an example, if the light source is coming from a DMD with a resolution of 1,920  $\times$  1,080 pixels, then the voxel map typically cannot have more than 1,920 and 1,080 voxels in the

X-direction and Y-direction, respectively, unless specialized hardware is used to allow the movement of the DMD-generated photomask in the XY plane<sup>40</sup>. The same principle applies to other light sources (as is the case for TPL, SLA and VAM), in which the resolution of the light is taken as the dimension of the voxel. Voxels can be assigned complex geometries, such as spheres, but for the purpose of vat-polymerization bioprinting, it is assumed that an individual voxel is usually given a cubic structure with a unitary value<sup>39</sup>. Several open-source software alternatives are available for voxelization in different programming languages, as listed in Supplementary Table 1.

**Slicing algorithms.** Once the 3D pixel map has been generated, as in when the input data have been voxelized, the next step is to transform the set of voxels into a technique-specific output by applying a technique-specific slicing algorithm (Supplementary Fig. 1). This is the crucial step that differentiates (from a software perspective) vat-polymerization techniques. As an example, TPL, SLA and DLP use a slicing algorithm wherein a defined number of voxel layers are grouped along the Z-axis and assigned a weight distribution to produce one image as an output<sup>6</sup>. The number of voxel layers that are grouped together is equivalent to the total number of bioprinted layers. New approaches have been developed to allow free-form bioprinting, in which the slice direction is not necessarily parallel to the Z-axis, but rather with variable normal vectors<sup>41</sup>. Although other slicing approaches exist for DLP-based techniques<sup>42</sup>, voxelization-to-slicing is a commonly used approach and several open-source software alternatives are available and analysed in Supplementary Table 1.

In the case of VAM, the slicing algorithm changes according to the specific volumetric fabrication approach selected. In the most common declination of this technology, tomographic bioprinting, the slicing is based on the Radon transform and Ram-Lak filter in the Fourier domain to the voxel map to obtain a set of images, which will then be filtered-back projected onto the vat<sup>32,33</sup>. New tomographic bioprinting slicing approaches to improve resolution have been developed wherein the first step is to apply a correction mask (attenuation correction, for example) and from there the same steps are followed<sup>43</sup>. It is worth mentioning that other technological solutions that belong to the VAM family, such as holographic printing<sup>15</sup> and xolography<sup>16</sup>, utilize DLP-like slicing algorithms whose synchronization also differs from tomography-based VAM techniques.

**Synchronization.** Once the desired output is obtained, the next step is to ensure the synchronization of all the different components; the most common being the control of a light source and a motor, dictated by the technique used and the available hardware. For DLP and VAM, as 2D images are projected, the only light source control needed is to specify the duration of exposure and to provide trigger signals<sup>6</sup>. Available software alternatives that facilitate the control of projected 2D images are Psychotoolbox-3 and slmPy for MATLAB and Python, respectively. Other techniques such as SLA have an additional step for the control of the light source; as an example, the tilt angle of a mirror is precisely controlled to direct the laser to specific points (*OpenExposer*). Trigger signals are also needed to specify the duration of light exposure. The light control for these techniques must be synchronized with a motor control, to enable 3D biofabrication. In TPL, SLA and DLP, the motor control is provided by a trigger signal and a specified distance and direction (provided by the desired layer height and selection of bottom-up or top-down approach)<sup>6</sup>. New approaches have been explored to continuously run in parallel light and motor to improve print speed<sup>44,45</sup>.

Other techniques such as tomographic bioprinting have a continuous rotating motor wherein the synchronization is defined by the speed at which the motor rotates and the refresh rate of the projected images<sup>32,33</sup>. As discussed previously, the synchronization that occurs in xolography<sup>16</sup>, though a subclass of VAM, is more closely related (from a software perspective) to that of continuous liquid interface production<sup>46</sup> than other volumetric printing methods. Finally, other peripherals can be added to the bioprinting system, such as sensors and monitoring systems<sup>16</sup>, additional light sources (dual colour)<sup>47</sup> as well as a temperature-controlled vat<sup>48</sup>.

## Bioresins

A broad range of synthetic monomer chemistries and functionalized biomacromolecules have been used in vat-polymerization-based bioprinting (Box 1). As with other strategies for 3D bioprinting, critical functional requirements must be satisfied by prospective bioresins regarding print stability, cytocompatibility and bioactivity<sup>18,49</sup>. However, emerging interests include incorporation of adaptable linkers and/or responsive groups to endow sophisticated 3D structures with more dynamic behaviours (such as mechanical transitions relevant to the native cellular microenvironment<sup>50</sup>) without compromising desired resolution and print speed.

**General considerations on printable materials.** Photopolymerization-based bioprinting is amenable to a multitude of bioresins, although complete access to very soft (<1 kPa) biomaterials has been limited by print stability. Specific properties of bioresins depend on the processing method. For example, SLA and DLP use low-viscosity bioresins, whereas TPL and VAM in general require comparatively more viscous formulations to limit blurring from diffusion of radicals and molecular components or sedimentation of the as-printed part<sup>51</sup>. Additionally, bioresin selection has an enormous impact on the pre-polymerization fluid properties, as common high-molecular-weight natural polymers are much more viscous even at low weight per cent (<5%) compared with the relatively low-molecular-weight synthetic macromers typically used in vat polymerization. Upon polymerization, user-specified material properties are highly dependent on applications, tissues and context<sup>52</sup> and can be further tailored with light-based crosslinking to construct gradients or other spatial variations in parameters such as stiffness, porosity and the concentration of network-tethered biomolecules<sup>53–55</sup>. Moreover, some newer types of bioresins are nanocomposites or microcomposites, incorporating particulate matter within an interstitial matrix<sup>36,56–58</sup>. These systems have integrated diverse materials, from inorganic or metallic (for example, silica, graphene, nanohydroxyapatite, gold and strontium carbonate) to polymeric (such as chitosan, cellulose, silk,  $\beta$ -lactoglobulin, micro-gels and emulsion droplets) fillers<sup>59–64</sup>. This growing class of composite resins increases functionality for diverse applications in directing cell differentiation, controlling release profiles or tuning mechanical properties; however, many of these formulations have yet to be applied in vat-photopolymerization bioprinting in particular with the presence of cells. Collectively, these techniques can be used to imbue vat-polymerized biomaterials with nuanced patterning of structure, mechanics, composition and stimuli-responsiveness.

**Crosslinking chemistry and green strength.** Cytocompatibility of the network-forming reaction dictates the success of vat-polymerization-based bioprinting applications. As a result, vat bioresins are typically formulated with poly(ethylene glycol) (PEG), gelatin or hyaluronic acid

macromers (macromolecular monomers) modified with various reactive groups. For more detailed discussion of specific formulations, we refer the reader to other in-depth reviews regarding photocrosslinkable bioresins<sup>12,22,36,37,52,65</sup>. Importantly, the kinetics of the bioresin crosslinking reactions must proceed at an adequate rate to prevent undesirable sedimentation of cells (the latter being a relevant consideration only for techniques in which the resin is in a reversible gel state, similar to gelatin, cannot be used), but also with mild reaction conditions to support cell viability. For photoinitiated polymerizations, some of the mostly commonly used macromers are PEGs, gelatin and hyaluronic acid functionalized with acryloyls or methacryloyls (chain polymerization) or thiols and norbornenes (step-growth polymerization)<sup>65</sup>. Important distinctions exist between these crosslinking chemistries and strategies for their photoinitiation. Typical bioresin photopolymerizations use 365-nm or visible light (including 405 nm) and water-soluble radical initiators, although specific initiation conditions vary by application and light source. Regardless, the concentration of radicals, cumulative light dose and incident photon energy must be restricted to a cytocompatible range. Type I photoinitiators (such as Irgacure 2959 and lithium phenyl-2,4,6-trimethylbenzoylphosphinate) undergo homolytic cleavage when irradiated, generating radicals; by contrast, excited type II photoinitiators (such as eosin Y and tris(2,2'-bipyridyl)ruthenium (II) chloride) do not fragment but rather produce radicals by hydrogen abstraction or electron transfer with co-initiating molecules<sup>66</sup>, rendering these slower and less efficient owing to competing reactions. However, co-initiation by tris(2,2'-bipyridyl)dichlororuthenium(II) hexahydrate/sodium persulfate (Ru/SPS) and visible light has been shown to result in improved cure depths compared with near-UV or visible-light-sensitive type I initiators<sup>67</sup>.

Chain polymerizations reach the gel point at low conversions (<2%), but are sensitive to oxygen inhibition, often require acryloyl-modified biomolecules for network functionalization and result in inhomogeneous, brittle networks<sup>22</sup>. By comparison, the thiol-ene and thiol-yne reactions form more homogenous, tougher networks<sup>68,69</sup>. These step-growth polymerizations require higher conversion to reach the gel point but are more oxygen-tolerant than chain polymerizations, rendering them very efficient. Moreover, thiol-reactive chemistries simplify network functionalization with biomolecules, as alkenes readily form thioether bonds with cysteine thiol radicals. Other bioorthogonal and initiator-free photoclickable, as well as some photooxidative, chemistries have also been applied to step-growth spatiotemporal hydrogel formation, but these are less common and introduce other challenges relating to synthesis and absorbance<sup>70–72</sup>. Recently, photooxidative tyrosine dimerization by Ru/SPS and visible light has been shown to be highly cytocompatible and capable of crosslinking native tyrosine residues in decellularized extracellular matrix (ECM)<sup>73</sup>, fibrin<sup>74</sup>, gelatin<sup>75,76</sup> and silk<sup>73,77</sup>, forgoing the need for macromer functionalization. Mixed-mode radical polymerizations (for example, thiol-acryloyl polymerization) have yet to be implemented in vat-polymerization-based bioprinting, but this chemistry provides distinct kinetics, mechanical properties and degradation profiles when compared with both step-growth and chain-growth polymerizations<sup>78</sup>. Various photochemistries can also be orthogonally and synergistically combined<sup>79</sup>. Next-generation tissue engineering research necessitates facile synthesis and scalability of photopolymerizable bioresins; in this respect, the thiol-ene reaction has been optimized for controlling physicochemical material properties while retaining superior cytocompatibility and kinetics over other radical-induced photopolymerizations<sup>80,81</sup>.

To further enhance post-polymerization stability, combinations of materials and chemistries have been used to create interpenetrating, dual-crosslinked or double networks by orthogonal light-triggered reactions<sup>82</sup> or non-photoinduced, dynamic self-assembly<sup>83</sup>. However, some studies have identified that self-healing, adaptable crosslinks can compromise shape stability in photopolymerized 3D structures, meaning that bioresin formulations containing dynamic bonds should be optimized to balance the benefits of self-healing

## Box 1

### Typical bioresin formulations for light-based vat-polymerization bioprinting

#### Hydrogel network materials

- Poly(ethylene glycol) derivatives
- Pluronic-F127 derivatives
- Poly(vinyl alcohol) derivatives
- Hyperbranched polyglycerol
- Decellularized extracellular matrix and derivatives
- Gelatin and derivatives
- Hyaluronic acid and derivatives
- Collagen and derivatives
- Silk and derivatives
- Alginate and derivatives

#### Photocrosslinking chemistries

- Acrylate and methacrylate chain polymerization
- Thiol-ene and thiol-yne step-growth polymerization
- Photooxidative tyrosine dimerization
- Initiator-free photoligation such as coumarin dimerization or diazonium photolysis
- Photoclick network conjugation of guest–host crosslinks

#### Small molecules and additives

- Photoinitiators such as I2959, LAP, Eosin Y, tris(2,2'-bipyridyl) dichlororuthenium(II) hexahydrate/sodium persulfate and upconverting nanoparticles
- Absorbers to limit light penetration or scattering
- Inhibitors such as scavengers or quenchers
- Refractive index modifiers such as iodixanol
- Nanocomposite components, for example, graphene or silica

#### Special considerations

- Ionic, hydrogen bonding or thermoresponsive components
- Dynamic, responsive or degradable macromers or crosslinkers
- Photocaged reactive groups
- Simultaneous preparation of interpenetrating networks
- Multimaterial approaches, for example, bioresin switching, overprinting or bioresin orthogonality
- Computed light-dose gradient for scattering correction
- Post-printing cell–material interactions such as network softening or contraction

with long-term print fidelity<sup>84–86</sup>. Similarly, green strength, or initial post-printing strength, of vat-polymerized biomaterials is important to consider and has been increased in DLP by inclusion of monomers containing ionic or hydrogen bonding sites<sup>87</sup>. Depending on post-printing reactivity (caused by unreacted functional groups), the final strength of the photopolymerized structures can be improved by flood curing or thermal annealing to induce additional crosslinking<sup>88</sup>. However, the initial and final mechanical properties are not always consistently reported and have yet to be compared across various vat photopolymerization techniques. By achieving near-quantitative conversion during the initial photopolymerization, some bioresins (such as thiol-ene formulations) avoid post-curing steps, but radical diffusion in such highly efficient systems can limit the resolution of bioprinted features.

**Reactivity, optical properties and viscosity.** As discussed, many existing photoinitiators have proven effective with cytocompatible light doses used in vat-polymerization-based bioprinting. Generally, the concentrations of photoinitiator and absorbers are on the order of millimolar or less with reactive functional group concentrations being tens to hundreds of times higher. This suggests that printing increasingly large 3D structures will mandate more efficiently absorbing initiation strategies and deeply penetrating wavelengths of light owing to intrinsic limitations imposed by optical thickness. Near-infrared-responsive and upconverting nanoparticles show promise for low-intensity, long-wavelength photoinitiation of common chemistries in bioresin crosslinking<sup>89,90</sup>, although the cytocompatibility of these methods has yet to be rigorously investigated. Combining photoinitiators with inhibitory molecules has improved feature resolution for some vat-polymerization applications, but also slows the overall reaction rate<sup>22</sup>. Although rapid reaction rates are desirable to minimize print times, kinetics must be tuned in accordance with light dose and radical diffusion, especially with reactions that are not oxygen-inhibited. For example, inclusion of the radical-scavenger 2,2,6,6-tetramethylpiperidin-1-yl)oxyl (TEMPO) was necessary for thiol-ene-based VAM of tubular structures, which otherwise could not be constructed without the TEMPO-mediated inhibition period<sup>91</sup>.

Photoabsorbers, which are usually non-reactive molecules containing chromophores that absorb light in the same range as the initiator, are used in bioresins to reduce light penetration depth, preventing overcuring and improving feature resolution. A broad range of photoabsorbers have been applied in light-based vat-polymerization bioprinting modalities, including Ponceau 4R, tartrazine, curcumin and anthocyanin, as well as nanohydroxyapatite and gold and melanin nanoparticles<sup>65,84</sup>. In recent examples, two-step absorption has been demonstrated with various mixtures of initiator, scavengers and quenchers, wherein an intermediate electronic state between the ground state of a photoinitiator and excited, radical-forming state is accessed in the one-photon pathway, overcoming restrictions of two-photon absorption in terms of both speed and resolution<sup>92,93</sup>. Alternatively, some absorbers are susceptible to photodegradation or photobleaching at specific wavelengths, allowing for other combinations of UV and visible light for 3D spatial control over photoinitiation<sup>44,94</sup>. Absorbers have also been shown to limit light scattering, which has alternatively been corrected for by continuous gradients in light dose<sup>43,95</sup>. Finally, optical properties have been directly tuned to account for scattering in cell-laden bioresins using refractive-index-matching compounds such as iodixanol<sup>34,96</sup>. Of interest, newer developments have further allowed light-based vat polymerization to occur in a radical (photoinitiator)-free manner,

by taking advantage of a caging/photoactivated uncaging process and photoclick reactions<sup>97</sup>.

Beyond the biomaterial components, cells are inherently light scattering, and cell sedimentation can lead to inhomogeneities in cell-laden bioprinted structures. Thus, high-molecular-weight photopolymerizable precursors or additives such as Percoll (colloidal silica) have been used to alter bioresin viscosity and reduce cell sedimentation<sup>22,52,98</sup>, and a buoyancy-assisted DLP system was developed to afford continuous-injection liquid interface polymerization and to avoid layering artefacts and cell settling during bioprinting<sup>99</sup>. Additionally, diffusion of reactive oligomers in liquid bioresins occurs on length scales that are obviously larger compared with feature sizes in DLP, creating conflicts when optimizing viscosity and extent of reaction<sup>100</sup>. By contrast, VAM can be extended to non-diffusive solid-state bioprinting for special bioresins, as with macromers capable of both thermogelation and photopolymerization<sup>101</sup>. Naturally, initiator concentration and light dose must be carefully balanced with the chosen bioresin formulation to achieve desired reaction kinetics, all while controlling viscosity and resolution (via inclusion of absorbers or inhibitors).

**Photodegradation and sacrificial materials.** TPL has been used to selectively cleave adhesive peptide linkers or degrade channels into pre-made hydrogels for perfusion or cell guidance using photocleavable moieties, such as nitrobenzyl, among others<sup>102–104</sup>. However, the strong absorbance of intrinsically photodegradable functional groups limits the maximum thickness of bioresins incorporating these chemistries, but certain strategies have exploited photoinitiation to induce degradation. For example, allyl sulfides and disulfides have limited intrinsic absorbance, but participate in bond scission cascades amplified by radical propagation, reducing the optical thickness and number of incident photons required for efficient de-gelation<sup>105,106</sup>. DLP and other vat-polymerization techniques have been utilized to generate degradable hydrogel and elastomer scaffolds to template contractile soft tissue constructs, perfusable vasculature and topographically defined intestinal stem cell monolayers<sup>107–110</sup>. Although photocleavable units have yet to be widely incorporated into bioresins for vat polymerization, other sacrificial (for example, hydrolytically degradable, enzyme-cleavable, thermo-reversible) or phase-separating components can be introduced for the production of high fidelity and intrinsically porous or vascularized 3D biomaterials<sup>63,64,111–113</sup>. Ultimately, light-based crosslinking of bioresins makes the fabrication of microscopically complex synthetic 3D tissues possible, with various possible formulations to optimize print fidelity and enable versatile post-printing modifications.

## Variations in techniques

**Bottom-up versus top-down configurations.** In SLA and DLP bioprinting, as 3D structures are formed eventually through a layer-by-layer method no matter, if within each layer, the pattern is created via raster-scanning or single exposure, different directions towards the layer-by-layer construction can thus be utilized. The bottom-up configuration pulls the construct up as a preceding layer is crosslinked, exposing the space between the layer and the vat bottom with the liquid bioresin for patterning of the next layer (Fig. 1c). Such a configuration is widely adopted, which confers the ability of 3D bioprinting with minimum bioresin usage and is convenient in most application scenarios. Nevertheless, because a bioprinted structure would need to be pulled upwards and out of the liquid bioresin as the crosslinked thickness increases, it would necessitate sufficient mechanical

properties of the bioresin in its crosslinked state to ensure integrity during the bioprinting process in combating the gravitational force. This dilemma is effectively addressed by switching the configuration to the top-down setup, in which the build plate is gradually moved downwards as each layer is patterned (Fig. 2a). As such, however, it is easily imagined that the vat must be deep enough to accommodate the entire thickness of the structure to be bioprinted, plus the depth of the build plate itself, leading to waste of bioresin. An additional disadvantage of the top-down configuration is the surface tension that may disturb the smoothness of the liquid bioresin between the preceding layer and air to be patterned, causing unwanted reduction in printing fidelity.

**Multimaterial bioprinting.** The ability to integrate multiple bioresins to introduce heterogeneity into bioprinted constructs is always instrumental to the engineering of structurally and functionally relevant tissues. Unlike nozzle-based or droplet-based bioprinting modalities, the unique requirement of successive operations within a vat for vat-polymerization bioprinting poses some limitations when one intends to achieve multimaterial fabrication. To date, multimaterial

vat polymerization has been achieved by several approaches<sup>6,114,115</sup>. One obvious solution is the use of multiple vats or similar configurations in SLA or DLP bioprinting<sup>116,117</sup> (Fig. 2b); as a layer of a different bioresin needs to be patterned, the previously bioprinted structure can be moved to another vat filled with the desired bioresin, with a washing process in a separate vat when switching back and forth. Alternatively, a single vat can be used with manual injection and depletion of different bioresins<sup>30,118</sup> or adopting a centrifugation approach to aid the removal of the bioresin during switching<sup>119</sup>. This set of methodologies is conceptually and instrumentally simple but is time-consuming owing to the numerous steps involved.

To streamline these various steps, alternatively, it has been shown that by introducing a microfluidic chip device into the system design in replacement of the traditional vat, it is possible to realize automated bioresin-exchange and washing procedures<sup>120,121</sup> (Fig. 2c), greatly improving the efficiency of multimaterial bioprinting. When a microfluidic chaotic mixer is further adopted either alone<sup>122</sup> or placed in front of the microfluidic chip device<sup>54</sup>, on-the-fly modulation of bioresin configurations or continuous gradients would be attainable. A more recent report proved the use of bioresins injected through

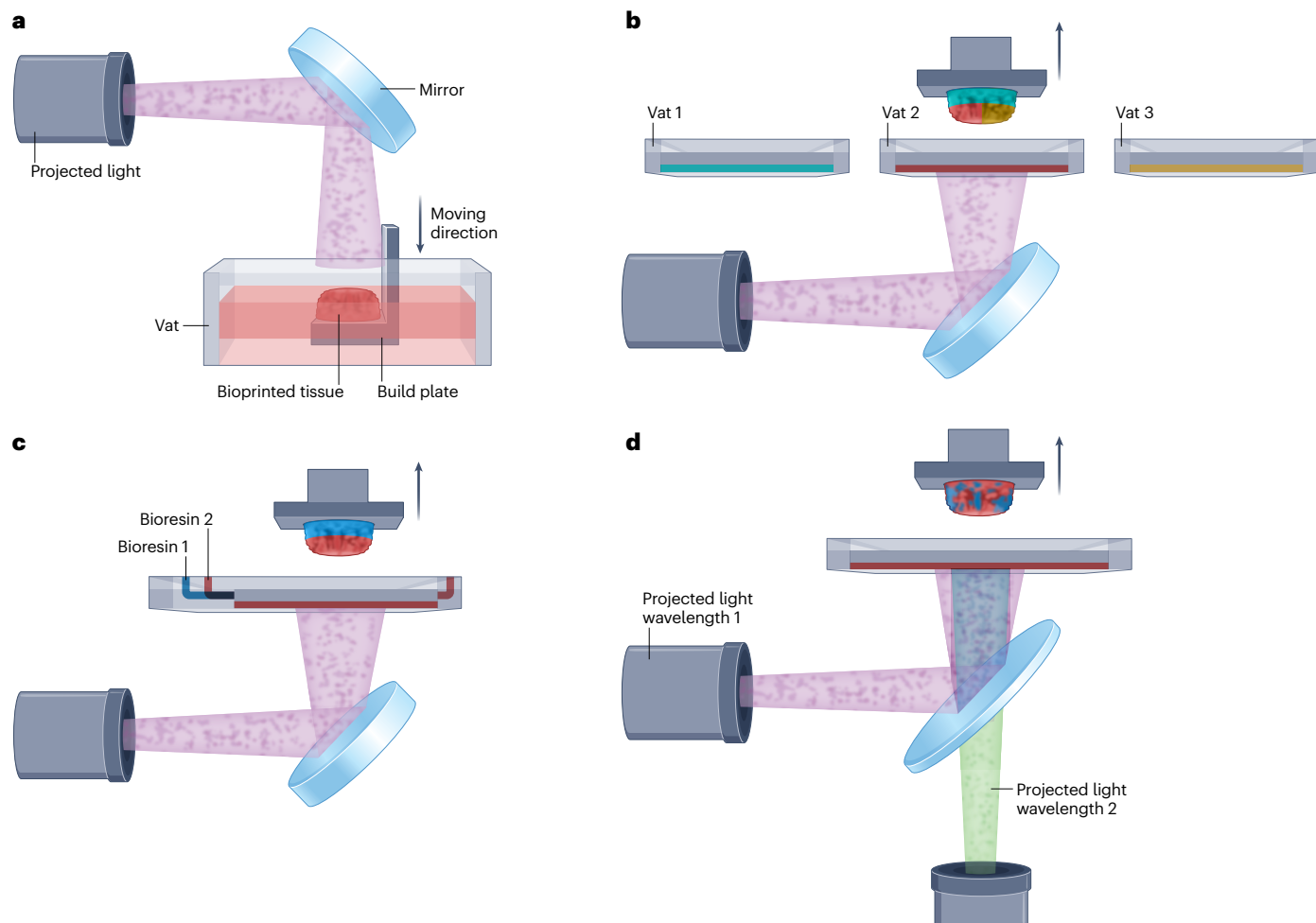


**Fig. 2 | Variations in vat-polymerization techniques, taking digital light processing bioprinting as an example.** **a**, Digital light processing (DLP) bioprinting in the top-down configuration. **b**, Multimaterial DLP bioprinting

using multiple vats. **c**, Multimaterial DLP bioprinting using automated bioresin change through a microfluidics-integrated vat. **d**, Heterogeneous-material DLP bioprinting using multiple wavelengths.

microfluidic channels dynamically created and integral to a printed construct to realize multimaterial DLP fabrication<sup>45</sup>. Despite that these multimaterial abilities are potentially transferrable to TPL or VAM, rare demonstrations have been reported mostly owing to the lack of moveable anchors for the photopatterned structures currently available in these modalities. Moreover, oftentimes, solid (physically gelled) bioresins are utilized in these two technologies to aid the bioprinting process, which naturally makes more complicated the possibility of multimaterial bioprinting, despite that multimaterial constructs having spatially separated zones can still be obtained by filling the vat with multiple bioresins in parallel<sup>123</sup>. Of note, one strategy of bioprinting with heterogeneous material properties that might be suitable for all the vat-polymerization methods discussed is that of taking advantage of the multi-wavelength bioprinting. This method was originally shown for simple photopatterning<sup>124</sup> then in DLP printing<sup>125,126</sup> (Fig. 2d), in which photoinitiators activatable under different wavelengths coupled with different photochemistries allowed crosslinking of specific components in a multicomponent bioresin vat, and was recently adapted for tomographic printing as well<sup>47</sup>. Similarly, greyscale fabrication using intensity-gradient photomasks is able to generate printed structures with mechanical property heterogeneities<sup>127,128</sup>.

**Converged approaches.** Each bioprinting technique has its own limitations, and thus there is a trend in the field of biofabrication to merge technologies and gain the advantages of two or more bioprinting modalities. For example, a DLP printer has been combined with an extrusion-based printer towards engineering interface tissues bearing unique property requirements for different segments<sup>129</sup>. DLP can also be integrated with jet printing to produce hybrid electronic devices<sup>130</sup> or with acoustic-assisted printing to achieve necessary alignments across the layers<sup>131–133</sup>. Within vat-polymerization bioprinting, both DLP<sup>134</sup> and tomographic printing<sup>135</sup> have been separately combined with TPL to enable 3D printing of constructs with feature resolutions across multiple scales, and tomographic printing has also been combined with melt electrowriting, to build fibre-reinforced structures<sup>136</sup>.

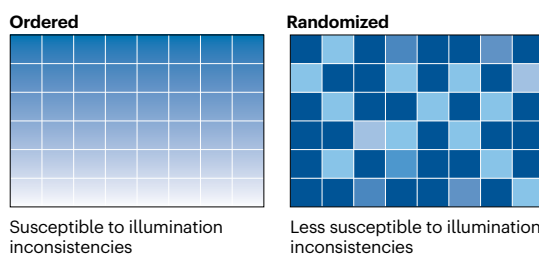
## Results

Light-based vat-polymerization bioprinting technologies enable the use of intricate designs for a rapid generation of complex bioprinted structures. Still, the generation of high-resolution structures with enhanced functionality, stability and mechanical properties requires optimization of used bioresins and different printing parameters such as light dose, print speed or layer thickness, depending on the used bioprinting technique. Even after successful bioprinting, freshly fabricated cell-loaded constructs have to mature into biologically functioning tissue equivalents. This requires material stability, biocompatibility and delivery of appropriate cell–material interactions guiding tissue morphogenesis, as well as specialized post-processing, culture and preservation conditions. Accordingly, the methods to assess printability parameters, resolutions and biological functioning and maturation of the bioprinted constructs are discussed.

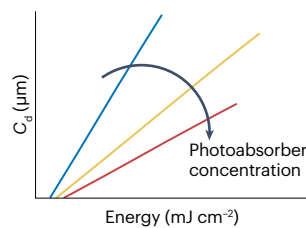
### Printability assessment

**Light-dose response and working curve generation.** In all light-based vat-polymerization techniques, printability and resolution are intimately dependent on the kinetics of the photocrosslinking reaction and therefore unique for each bioresin formulation<sup>84</sup>. A key parameter to be optimized and enabling printability is the amount of light energy (dose) that is supplied to each voxel. Too low doses lead to insufficient crosslinking and failure to develop the smallest feature sizes, whereas too high doses can lead to over-crosslinking and loss of resolution owing to off-target polymerization<sup>111,137</sup>. In the context of SLA and DLP, therefore, a first step is to assess the relation between different irradiation conditions and the spatial propagation of the polymer crosslinking within the bioresin vat, a relation estimated by the working curve for the given photopolymer. A simple method to establish the SLA or DLP working curves consists of projecting onto the bioresin vat an array of spaced disks or squares, with each sample exposed to an increasing light dose (Fig. 3a). The irradiation pattern can also be randomized to minimize the effect of possible unequal illumination across the build window<sup>138</sup>. For higher light doses, light will travel further into

#### a Light-dose determination

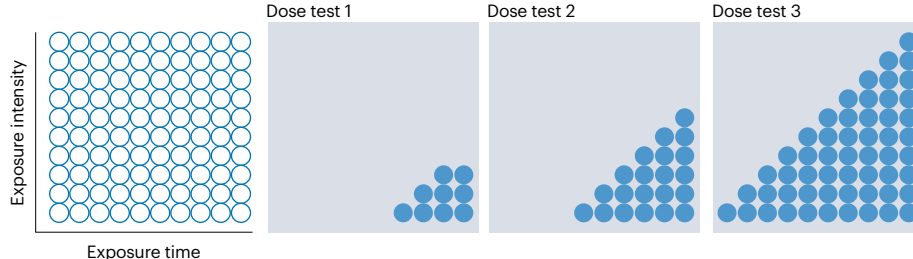


#### b Light-dose versus photoabsorber concentration



**Fig. 3 | Determining light-dose responses and working curves in light-based vat-polymerization bioprinting.** **a**, A simple method to establish the single-photon stereolithography or digital light processing working curves consists of projecting an array of disks or squares onto the bioresin vat where each of those is exposed to an increasing light dose. **b**, After crosslinking, the thicknesses of the bioresin layer are measured and recorded to create a light energy versus thickness plot that can be used to construct the working curves. **c**, A dose test is performed to identify ideal light-exposure parameters for tomographic bioprinting, by projecting an array of disk-shaped spots within a cuvette containing the bioresin, with each spot corresponding to a varying light intensity and exposure time.  $C_d$ , curing depth; VAM, volumetric additive manufacturing.

#### c Determining light dose in VAM



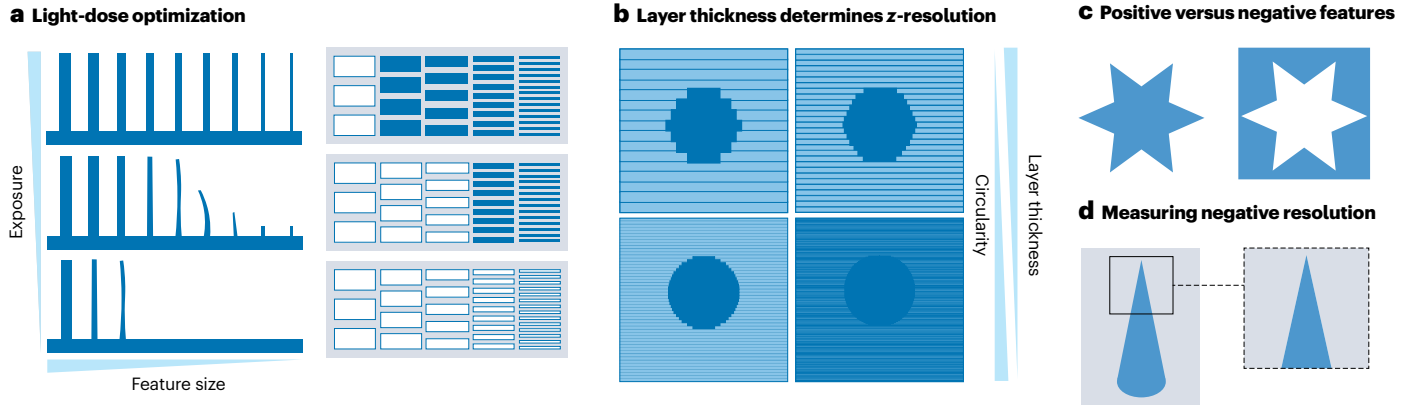


**Fig. 4 | Resolution assessments in light-based vat-polymerization bioprinting.**

**a**, In point-by-point and layer-by-layer vat polymerization, resolution is assessed by printing diagnostic models with small positive and negative features that range in size at light-exposure parameters in the optimal range identified with the working curve. **b**, In single-photon stereolithography and digital light processing, the printed structures can display a notable pixelated profile depending on the

layer thickness. **c**, Tomographic bioprinting enables fabrication of objects in a layerless fashion with the resolutions measurable through attainable negative and positive features. **d**, Measurement of the resolution of negative features can be facilitated by using fluorescent dyes; here a negative cone is filled with a dye, and the maximum attainable negative resolution is determined by measuring the tip dimensions of the cone.

the bioresin (curing depth,  $C_d$ ), causing the crosslinking of a thicker structure. After irradiation, the uncured bioresin is washed off. Depending on the stiffness of the resulting hydrogel constructs, and on how close to each other these have been crosslinked, their thickness can be measured with a caliper, a profilometer, a micrometre or from microscopy images and then recorded to create a light energy versus thickness plot (Fig. 3b). The working curve is then defined by the following equation, where  $D_p$  indicates the light penetration depth and  $E_c$  indicates the minimum energy needed to crosslink the photopolymer:

$$C_d = D_p \cdot \ln \frac{E}{E_c} \quad (1)$$

This information is crucial to select the photoexposure condition and the layer height that can be targeted when bioprinting (and therefore the highest resolution achievable in the Z-direction, or axial resolution). However, it should be kept in mind that, in practice, the light intensity is not perfectly uniform throughout the thickness of the layer<sup>139</sup>. The light intensity tends to drop off as it moves through the bioresin owing to absorption effects, and therefore the layer starts crosslinking closer to the light source and grows in thickness over time during the photoexposure step, until it reaches the previously crosslinked layer. Therefore, to ensure effective binding of a layer onto the previous one, exposure time should be slightly increased above what is identified according to the working curve. The exact light dose (and layer height) can be fine-tuned empirically with test prints.

In tomographic bioprinting, identification of the workable light dose range is the first step towards printability. As this approach is layer-free and, in principle, all the parts of the object are crosslinked at once and near-simultaneously, a key parameter governing printability is the threshold energy needed to initiate photocrosslinking, which can also be detected with a dose test, similar to those classically used in TPL optimization<sup>140</sup>. Typically, an array of disk-shaped spots is projected across the build volume, in which a static, non-rotating square cuvette containing the bioresin is placed (Fig. 3c). Each spot corresponds to a given light intensity and exposure time (usually varying from a

few seconds to no more than a couple of minutes). In tomographic bioprinting, different from SLA and DLP, light needs to travel all the way through the vat in the direction longitudinal to the projections, with at least 37% of the incoming light intensity reaching the opposite edge of the vat<sup>139</sup>. Thus, rather than measuring the  $C_d$ , the lowest dose required to obtain a crosslinked disk that bridges the entire thickness of the cuvette is recorded as needed to ensure printability<sup>80</sup>.

**Resolution assessment.** Resolution in light-based vat polymerization directly correlates with the capacity of the bioprinting process to confine the photocrosslinking reaction within the desired voxel and therefore is correlated to the optical voxel size (for example, size of the laser spot or of the pixels on the DMD), the light-dose distribution inside and outside the voxel of interest and the mobility and diffusion of the reactive species triggering the crosslinking<sup>109</sup>. Resolution also differs depending on the axis along which it is measured in the produced object (as in longitudinal or orthogonal to the direction of projection of the light) and if the measurement refers to positive features (such as spikes, tips and pillars) or negative features (such as channels, pores and voids)<sup>141</sup>. Typical assays to assess resolution in layer-by-layer vat polymerization consist of printing diagnostic models with small positive features, such as rectangular posts ranging in size at light-exposure parameters in the optimal range identified with the working curve. At decreasing exposure, the smaller positive features are not formed and with half the light energy only the largest ones will form but they will be weaker and thinner than they should be. However, simply maximizing exposure leads to overprinting<sup>142</sup>. This is especially relevant for printing negative features: when printing gaps of different sizes, high-exposure printing will resolve the larger gaps but will lead to complete fill-in of the smaller ones effectively lowering the resolution (Fig. 4a). More notably, in point-by-point and layer-by-layer methods, the axial resolution, longitudinal to the light projection, is determined by the layer thickness. Overcuring utilizing too high light doses can therefore lead to difficulties in printing overhangs and pores oriented along the XY plane, as if the  $C_d$  is longer than the layer height; pores in the adjacent layers will be clogged by partly

crosslinked bioresins. All these effects can be quantified by printing at different layer thickness test models, such as cubes with longitudinal pores (of cylindrical or squared section) of different sizes<sup>143</sup>. Finally, as each layer is composed by joined rectangular voxels, the surface of the printed objects can display a pixelated profile, which can be readily evaluated through microscopy images, depending on the resolution of the device<sup>144</sup>. For the same region, cross-sections of the object to be printed can also reveal a clear layering pattern that depends on the layer thickness (Fig. 4b). Although this printing artefact could also be exploited to introduce roughness useful for aligning cultured cells via contact guidance, continuous bioprinting approaches, such as continuous liquid interface production and xography, can be used to minimize their appearance<sup>145</sup>.

In tomographic bioprinting, the planar axis, which is perpendicular to the direction of light, and the tomographic axis, which is parallel to the direction of light, have different phenomena that are governing their resolution. The surface of the DMD is imaged into the vial containing the material. The voxel resolution in the centre of the build volume is determined by the pixel size of the modulator and the magnification of the lens system. However, at a distance from the centre of the printed object, the effective pixel size increases proportionally to the divergence of the illumination beam. The etendue of the illumination source and the accuracy of the volumetric dose reconstruction lead to decrease in resolution, which can be limited by using illumination source with a low etendue<sup>146</sup>. In addition, overall resolution might be affected by the diffusion of radical species and sedimentation of the printed object<sup>147</sup>. Use of the bioresins with high viscosities (>10 Pa s) counteracts the sedimentation of the printed object below 10 µm (ref. 146), an effect that can be even negated by the use of thermoreversible gelling materials such as gelatin. Moreover, highly viscous resins also limit the diffusion of the radical species outside the voxels of interest<sup>33</sup>. Resolution assessment is performed by printing the object with positive and negative features (Fig. 4c), which can then be analysed with microscopy<sup>34</sup>. To facilitate visualization of small negative features and to improve their imaging contrast, the hydrogel bioresin can be formulated with a fluorescent dye or oppositely the hollow object can be filled, for instance, with fluorescent dye (Fig. 4d).

**Metrology, image reconstruction and imaging techniques for characterizations.** An initial printability assessment during the printing process is done using a monitoring camera. After the sample is printed, it can be inspected visually and using simple stereomicroscopy. For a more precise analysis, microcomputed tomography can be performed to reproduce full sample architecture. Alternatively, printed objects can be scanned in 3D with resolutions down to 0.01 mm or imaged using a light-sheet microscope, confocal microscope or a fluorescent microscope equipped with computation clearing. The imaged 3D object can be reconstructed using microscope-specific software such as LAS X (Leica) or ZEN (Zeiss) or open-source software such as ImageJ or nRecon and after correction of light distortion in the z-dimension, the image can be reconstructed in 3D. For specific analysis, the reconstructed sample morphology can be compared with the original 3D model of the object using ImageJ plugins or specified software such as Cloudcompare. These software tools compare the STL file of the model with that of the bioprinted sample and calculate the differences of the volume fidelity between them, giving the sample-to-model fidelity in percentage. For example, volumetric bioprinting shows on average volume variation of below 5–10% when comparing the

printed constructs acquired via microcomputed tomography and the original STL files<sup>33</sup>.

**Cellular assessment.** The bioprinted constructs can be stored, cultured and analysed similarly to cell-laden photocurable hydrogels, which are frequently used as 3D culture systems<sup>148</sup>. In contrast to extrusion-based bioprinting<sup>18</sup>, light-based vat-polymerization bioprinting techniques are nozzle-free and do not impose high shearing forces on the encapsulated cells avoiding destruction of cluster architectures, organizations and cell-cell interactions<sup>34</sup>. Typically, the use of light-based polymerization, especially in the UV-A and near-UV visible-light range, together with free-radical generation common to many photo-chemistries used in vat polymerization, may raise concerns regarding potential cell impairment, and therefore assessments evaluating the presence or absence of DNA damage or oxidative stress can be beneficial<sup>149</sup>. It should also be noted that previous literature has extensively reported safe photoexposure windows of parameters, in which no lasting cell impairment is found even with the proteome analyses<sup>150</sup>, and that photoreactive hydrogels can protect the cells from free radicals, as the radicals are captured to trigger crosslinking reactions, such as in chain-growth polymerization<sup>151</sup>. Additionally, the maturation capacity of the encapsulated cells demonstrates compatibility of bioresins, bioprinting process and subsequent culture conditions, which takes place over several days to weeks, in some cases even months. In the case of organoids or stem cell clusters, maturation is demonstrated by the ability of the encapsulated cells to differentiate and to form highly organized structures resembling the natural architecture of the target organs<sup>152</sup>. Advanced maturation is associated with obtaining organ-specific functionality, such as measuring the electrophysiology in stem-cell-derived neuronal cells<sup>110</sup>, and ability of ammonium elimination from perfusate for liver organoids<sup>34</sup>.

## Applications

Light-based vat-polymerization bioprinting represents a promising technology for a wide range of biomedical applications. This section offers an overview of the various strategies exploited for engineering structurally and physiologically relevant tissues towards regenerative medicine and tissue models for use in drug discovery.

### Point-by-point scanning

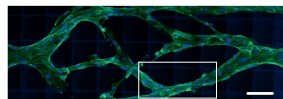
Two-photon irradiation can be exploited in multiple ways, from polymerizing 3D scaffolds<sup>22,153–156</sup> and patterning them with bioactive molecules<sup>53,157–160</sup> to degrading them by means of photocleavage reactions<sup>103,161,162</sup> or ablation<sup>135,163,164</sup> (Fig. 5A). However, owing to the limited build volume and long printing process, TPL has been so far largely limited to constructs ranging from hundreds of micrometres to few millimetres<sup>22,153</sup>. This limits the ability of TPL to target tissue size or organ size, but it holds great promises for high-precision bioprinting of microtissue models<sup>97,135,154,155,162,165–167</sup>, production of soft microstructured cell and drug delivery systems (such as microneedle arrays or microrobots)<sup>168–172</sup> and the study of cell mechanobiology<sup>173,174</sup>. Moreover, owing to the intrinsic confocality of two-photon irradiation and enhanced tissue penetration of near-infrared wavelengths, TPL has also been explored for printing *in vivo*<sup>175</sup> and inside (synthetic) cells<sup>176</sup>.

### Layer-by-layer projection

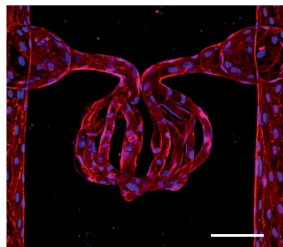
Projection-based lithography has been used with various cell types, such as stem cells and their derivative cell types<sup>30,55,110,177</sup>, mesenchymal stem cells<sup>54,178</sup>, adipose-derived stem cells<sup>179,180</sup>, endothelial cells<sup>54,55,178,181,182</sup>,

## A Point-by-point

**Aa**



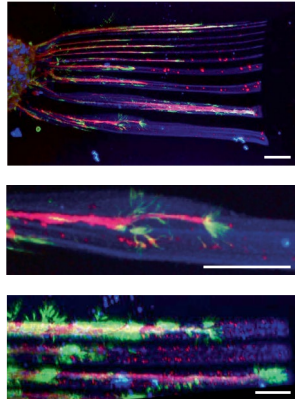
**Ab**



**Bb**

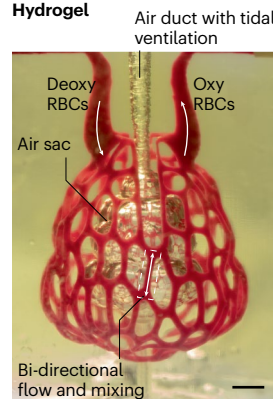


**Ac**

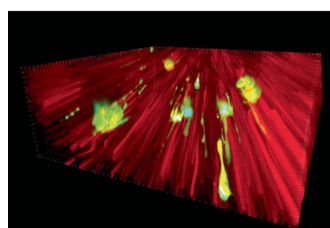


## B Layer-by-layer

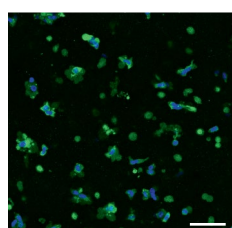
**Ba**



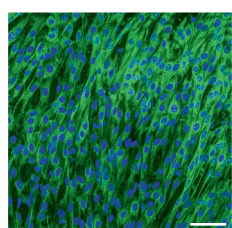
**Bc**



**Bd**



GH      Hase

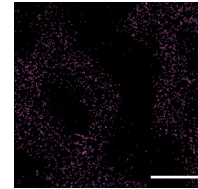


## C Volumetric

**Ca**



**Cb**



**Cc**

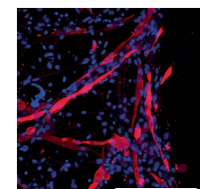
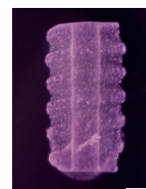


## Fig. 5 | Examples of tissue-engineered constructs.

**A**, Examples of point-by-point printing. **Aa**, Point-by-point printing of vascular network by means of two-photon mechanism with human umbilical vein endothelial cells endothelialization. F-actin (green) and nuclei (blue). Scale bar, 100 µm. **Ab**, Two-photon-based ablation and endothelialization of glomerulus-like vasculature. Scale bar, 100 µm. **Ac**, Two-photon patterning of growth factors to guide axon outgrowth. Avidin-SAT-F + NGF (blue), BIII-tubulin (red) and F-actin (green). Scale bar, 50 µm. **B**, Examples of layer-by-layer printing. **Ba**, Layer-by-layer printing of entangled vasculature networks. Scale bar, 1 mm. **Bb**, Fast printing of large constructs featuring perfusible channels. Scale bar, 1 cm. **Bc**, Cellular alignment in FLight-bioprinted constructs at day 1 (top) and day 7 (bottom). Filamentous gel (red), normal human dermal fibroblasts (green) and nuclei (blue). Scale bars, 20 µm. **Bd**, Differentiation of C2C12 muscle cells in bioprinted constructs without (stiff gel, gelatin + hyaluronic acid methacrylate (GH)) or with (soft gel, hyaluronidase (Hase)) enzymatic digestion. Myosin heavy chain (green) and nuclei (blue). Scale bar, 50 µm. **C**, Examples of volumetric printing. **Ca**, High-fidelity tomographic printing of mouse pulmonary artery. Scale bars, 5 mm. **Cb**, Bioprinting of mesenchymal stem cell-laden trabecular bone. Osteogenic medium-primed mesenchymal stem cells (pink). Scale bars, 2 mm and 500 µm. **Cc**, Bioprinting of C2C12 myoblast-laden complex model. Myosin heavy chain (red) and nuclei (blue). Scale bars, 2 mm and 200 µm. RBC, red blood cell. Part **Aa** reprinted with permission from ref. 160, Wiley. Part **Ab** reprinted with permission from ref. 163, Wiley. Part **Ac** reprinted with permission from ref. 158, Wiley. Part **Ba** reprinted with permission from ref. 143, AAAS. Part **Bb** reprinted with permission from ref. 191, Wiley. Part **Bc** reprinted from ref. 201, CC BY 4.0. Part **Bd** reprinted from ref. 110, Springer Nature Limited. Part **Ca** reprinted from ref. 146, Springer Nature Limited. Part **Cb** reprinted with permission from ref. 33, Wiley. Part **Cc** reprinted with permission from ref. 80, Wiley.

myoblasts<sup>54,183</sup>, hepatic cells<sup>184–186</sup>, chondrocytes<sup>187</sup> and tumour cells<sup>188</sup>, showing good biocompatibility (cell viability  $\geq 70\text{--}80\%$ ), thus opening the way to various tissue targets.

Of pivotal importance for the successful engineering of large tissue constructs, DLP has gained particular interest for the generation of multiscale vasculature networks<sup>111,189</sup>. This has been elegantly demonstrated by the generation of 3D entangled vascular networks resembling alveolar topology<sup>143</sup> (Fig. 5Ba). In vitro and in vivo studies confirmed the potential of this method to generate large, vascularized tissues for regenerative medicine. This technology, acquired by 3D Systems, has progressed towards full size lung constructs with micron-level capillaries and is heading towards preclinical transplantation studies in collaboration with Lung Biotechnology PBC (United Therapeutics)<sup>190</sup>. Also recently, the high-fluidity-photoresin approach was leveraged to bioprint large, clinically relevant-sized cell-laden hydrogels featuring vessel networks (Fig. 5Bb), thus maintaining high cell viability in the core of the construct owing to improved nutrient and oxygen transport<sup>191</sup>.

Besides vascularized constructs, DLP holds great promises for the printing of a wide variety of other cell-laden implants and tissue models. For example, it has been used to bioprint cartilage<sup>179,187,192</sup>, bone<sup>193</sup>, corneal<sup>180</sup>, glioblastoma and liver-like tissues as well as acellular heart valves<sup>194</sup>, bone implants<sup>195,196</sup>, vascular grafts<sup>197</sup> and nerve conduits<sup>198–200</sup>. Another DLP-enabled technology termed filamented light (FLight) biofabrication has also recently emerged as a promising method to bioprint aligned tissue constructs with unprecedented speed and cell guidance capabilities<sup>201</sup> (Fig. 5Bc). In addition, DLP has been explored for non-invasive, *in vivo* bioprinting. In contrast to the conventionally used 365–405-nm irradiation, the higher tissue penetration capacity of near-infrared light (980 nm) was exploited to photocrosslink 3D structures *in situ* within subcutaneously injected photoresin<sup>202</sup>. Interestingly, DLP can be exploited to manufacture programmable shape-morphing hydrogel constructs (4D printing), thus making it possible to obtain complex 3D geometries and curvatures from relatively simple prints<sup>203,204</sup>.

ECM and cellular heterogeneity strongly contribute to the mechanical and physiological functions of human tissues. Using a nitrobenzyl-modified chondroitin sulfate to mitigate excess of free radicals diffusion, high-resolution, multicellular bioprinting of liver units was reported<sup>186</sup>. In other examples, geometric complexity was combined with regionally varied stiffness<sup>184,205</sup> or with post-printing patterning of bioactive molecules<sup>55</sup>, thus further improving the functionality of the biomimetic cell microenvironment. Cell spreading and nutrient exchange can be modulated and improved with the use of bioresins containing porogens, which is of particular importance for large tissue constructs<sup>54,63,64,111,113</sup>.

Overall, projection-based bioprinting offers an unprecedented opportunity to biofabricate large, yet highly complex tissue architectures. However, to date, high resolution has been generally achieved with highly concentrated photoresins (typically  $>10\%$  gelatin methacryloyl (GelMA) or PEG-diacrylate), thus resulting in stiff constructs. Recently, a post-printing molecular cleavage approach was proposed to tune the mechanical properties of the bioprinted constructs without affecting their structural complexity<sup>110</sup>, opening new avenues for DLP-based bioprinting of ultrasoft tissues (Fig. 5Bd).

## Volumetric approaches

Despite being in its infancy, tomographic printing has been already explored to generate vascular-like constructs<sup>77,146,206</sup>, as well as bioprinting of tissues resembling cartilage<sup>33</sup>, muscle<sup>80</sup>, liver<sup>34</sup> and bone<sup>206</sup>

(Fig. 5C). The rapid fabrication times and the absence of mechanical stresses imposed to cells can be particularly beneficial for applications in which fragile cellular structures (such as epithelial organoids) are involved<sup>34</sup>. Contrary to SLA and DLP, tomographic bioprinting requires high photoresin transparency for the light to penetrate through the whole printing volume. This aspect intrinsically limits the number of suitable photoresins, as well as the density of embedded cells (typically  $<2 \times 10^7 \text{ cells ml}^{-1}$ ), if strategies that mitigate light scattering caused by intracellular organelles are not in place. In particular, low cell densities are less desirable as the biofabrication field moves towards increasingly high cell density bioinks and bioresins (tens or hundreds of million cells per millilitre)<sup>207</sup>. With current capabilities, tomographic bioprinting is a manufacturing method better indicated to generate relatively low cell densities, centimetre-scale tissue constructs, free-form soft robotics components and perfusable tissue models for organ-on-chip technology. Substantial advances for tomographic bioprinting competitiveness could result from the introduction of multimaterial/multicellular printing strategies<sup>123</sup>, elimination or enabling to design self-focusing-induced microporosity<sup>135,208</sup> and further improvement of positive and negative resolutions that are to date generally equal or lower to SLA and DLP.

## Reproducibility and data deposition

Several factors can influence the reproducibility of vat-polymerization bioprinting processes and the quality of resulting bioprinted tissue constructs. To ensure extended applications of these bioprinting techniques, considerations in a multitude of parameters such as bioink designs and preparations, operational procedures as well as data reporting and repositories shall be carefully taken.

## Bioresin considerations

As photoactivatable bioresins are key to any of the light-based vat-polymerization bioprinting techniques, the biomaterials oftentimes would need to be functionalized from their pristine forms to be usable. Synthetic biomaterials are usually more reproducible especially those that can be commercially sourced that have undergone proper quality controls. Naturally derived biomaterials, on the contrary, can be quite inconsistent in their reproducibility owing to multiple reasons. One is the nature of these biomaterials; as they are produced from natural tissues, depending on the species and tissue type they are coming from, as well as their processing method, the raw, unmodified biomaterials are already inconsistent in their properties made up of molecules of varying molecular weights and molecular sequences or configurations, in particular with protein-based biomaterials. Then, with further functionalization to endow these biomaterials with photoactivatable moieties, which involves additional processing steps, more variabilities may be introduced leading to quality concerns for these naturally derived biomaterials when they are used as bioresins for bioprinting.

Some new developments have shown the potential to simplify the problem, to some degree. For example, the relatively recently reported photoinitiator of Ru/SPS<sup>74,75</sup> enables efficient formation of crosslinks through oxidizing aromatic residues such as those in tyrosine leading to generation of di-tyrosine bonds with adjacent tyrosine groups. Accordingly, protein biomaterials in their unmodified form can be directly photocrosslinked as long as sufficient tyrosine groups are present on their molecular chains, such as fibrin<sup>74</sup>, gelatin<sup>76</sup>, decellularized ECM<sup>73</sup> and silk<sup>75,77</sup>, among others.

Incorporation of cells poses another major factor contributing to reproducibility issues. Beyond the cell-source variability that is

universal to any biofabrication methods, the cell type and density also matter in terms of determining bioresin performances owing to the light-based production procedures that are easily impacted by scattering and diffraction of incident light. A recent publication indicated that by introducing cytocompatible refractive-index-matching compounds such as iodixanol, VAM<sup>34</sup> or DLP<sup>96</sup> bioprinting in the presence of high cell densities is possible without remarkably sacrificing the resolution. Another concern is the sedimentation of the cells during the bioprinting process, which can be addressed in TPL and VAM using physically gelled solid bioresins, which, nonetheless, remains as a major obstacle for SLA and DLP bioprinting as liquid bioresins would have to be used in these setups.

## Other operational considerations

Although the effect of bioresin viscosity is not as strong as in some other bioprinting methods such as extrusion (which uses high viscosity values) and inkjet (which uses low viscosity values), it is also a factor to consider in vat-polymerization techniques. TPL when it comes to photocrosslinking as well as VAM, as discussed earlier, can accommodate wider ranges of bioresins as both liquid and solid bioresins can be used towards fabrication as long as the structures are anchored to the surface of the build plate. For photodegradation of TPL, by contrast, it has to start with solid bioresins, given the fact that the patterned free-form hollow structures need to be mechanically supported to avoid shape change. For SLA and DLP bioprinting, the bioresins need to be in the liquid form; however, a wide range of bioresin viscosities can be used (10–5,000 mPa s). It is important to note that parameters such as

ambient temperature could affect the reproducibility, especially for temperature-sensitive bioresins such as those based on gelatin. To this end, the utility of fish gelatin and its derivatives shows advantages owing to their lower responsiveness to temperature compared with porcine counterparts<sup>111</sup>.

Bioprinter hardware and software further contribute to the reproducibility performance of vat-polymerization platforms. Examples include control precision such as that for motor movements in the XY plane (for raster-scanning mode), the Z-direction (for both point-by-point and layer-by-layer scanning modes) and the rotation (for tomographic printing). However, unless the systems are custom-built, the freedom of such controls is always limited when commercial bioprinters are used. Unlike extrusion bioprinting, path planning may not aid much in vat-polymerization bioprinting.

## Reporting and data repositories

Standardization in bioresins and experimental procedure are lacking for vat-polymerization bioprinting, and reporting standards are rarely considered by the community. In Box 2, we list a collection of key items that must be reported to ensure that sufficient information is included to promote reproducibility. Databases for vat-polymerization bioprinting – or bioprinting in general – are scarce. The [3D Printing Database](#) is dedicated to 3D printing and bioprinting collectively, yet the number of parameter items is still very limited, and entries are not classified by printing or bioprinting modalities, which require distinct sets of reporting parameters for their operations (see those necessary for extrusion bioprinting<sup>18</sup>). [GitHub](#), a repository of software

## Box 2

### Recommended reporting standards

#### Bioresins (biomaterials)

- Type of biomaterial
- Origin of biomaterial
- Biomaterial concentration
- Catalogue or lot number of biomaterials (if commercially sourced)
- Procedures for synthesis, derivation or modification of biomaterials (if manufactured in-house)
- Pertinent information regarding photoinitiators

#### Bioresins (cells)

- Type of cell or cells
- Catalogue or lot number of cells
- Cell-culture medium and conditions
- Passage number
- Cell density
- Procedures for isolation, modification or differentiation of cells (if applicable)

#### Bioprinter hardware and software

- Type/model
- Subtype
- Bioresin/vat temperature
- Specifics for DIY or modification (if applicable)

#### Bioprinting procedure

- Raster-scanning step size (two-photon mechanism (TPL)/single-photon lasers (SLA)) or projection pixel size (digital light processing (DLP))/volumetric additive manufacturing)
- Raster-scanning speed (TPL/SLA), layer projection time (DLP) or vat rotation speed (volumetric additive manufacturing)
- Layer thickness (TPL/SLA/DLP) or vat rotation step angle (tomographic printing)
- Details of software used for segmentation and planning the bioprinting path; specify if custom-designed
- Ambient temperature if different from that of bioresin/vat
- Other photocrosslinking or photodegradation parameters, including laser/light output power density and wavelength used. If multiple procedures are used (such as in multimaterial), specific information of each procedure shall be reported

#### Post-bioprinting

- Tissue culture conditions
- Maturation conditions
- Specifics on culture medium, culture container and other culture conditions
- Type and specifics of the maturation methods if applicable, for example, flow, biomechanical or bioelectrical

## Glossary

### Green strength

The strength of the 3D-bioprinted material before it is processed to its final strength.

### Melt electrowriting

A 3D printing method that uses electric fields to draw molten polymer filaments at microscale or nanoscale diameters with defined patterns before bending instabilities occur.

### Multi-wavelength bioprinting

Bioprinting using multiple wavelengths, where each wavelength crosslinks a specific component within the bioresin.

### Porogens

An additive that can disperse in the bioresin and may leach out or dissolve away to form pores in the material.

and firmware version-control and collaboration platform, may also be useful for vat-polymerization bioprinting. In general, a trend is that databases for open scientific and research data-sharing are becoming increasingly more common, with examples being [Zenodo](#) and [Mendeley Data](#), among others.

## Limitations and optimizations

Different vat-polymerization bioprinting techniques have their own unique advantages and disadvantages, resulting in the different ranges of key performance indicators that each of them can achieve towards various applications in tissue fabrication (Table 1). In this section, some major limitations of these vat-polymerization bioprinting techniques are discussed with potential solutions to optimizations also suggested.

### Mechanical property–gravity balance

SLA and DLP bioprinting can be divided into top-down and bottom-up configurations. Although the former is not quite influenced by gravitational force during the 3D construction process as the platform is always immersed within the liquid bioresin, it is plagued by surface tension problems as well as the substantial waste of the bioresin. On the contrary, the bottom-up approach uses the minimal bioresin possible, but as the upward-pulled parts often are exposed to air out of the liquid bath, it is difficult to maintain integrity of the bioprinted structures when soft tissues need to be engineered. Several methodologies have been proposed accordingly. In one example, a fluid support was utilized to introduce buoyancy force in mitigating the force caused by gravity, during the pulling steps<sup>99</sup>. Alternatively, the bioresins can be meticulously designed, such as using a multicomponent bioresin of GelMA and hyaluronic acid methacrylate, which enable stiff constructs to be created initially, followed by subsequent selective cleavage of the hyaluronic acid methacrylate molecules to return the mechanical properties back to those controlled by the low-concentration GelMA<sup>110</sup>.

### Addressing limitations of reconstruction

Of all the techniques belonging to the family of vat polymerization, tomographic bioprinting is one of the most recent. How, and, albeit promising, it is still in its infancy. Further research efforts are required to advance this technique. In terms of software and reconstruction algorithms, the current versions are directly derived from processes commonly utilized in tomographic imaging, in which the filtering and back-projection steps produce a virtual image, rather than a physical object. The Ram-Lak filter returns projections with both negative and

positive values, the former of which would require sending light capable of inhibiting the crosslinking reaction. Although this concept has been already demonstrated<sup>209</sup>, the practical implementation is not trivial, and current algorithms circumvent this challenge by thresholding and setting the negative values to zero. As this results in the accumulation of high undesired light doses in certain off-target regions of the design, in some cases, it could partly overcure thin features, therefore reducing the achievable resolution. Although algorithms including corrections to improve contrast between on-target and off-target regions of the vat are being successfully developed<sup>146,210</sup>, further research in printing-dedicated tomographic reconstructions is needed to maximize the resolution of tomographic bioprinting. This is also especially relevant for the field of bioprinting, in which the accuracy of the tomographic printing process can be hampered by light scattering caused by cells, microparticles and ECM aggregates. Methods to adjust the refractive index of the bioresins with biocompatible index-matching compounds and to computationally minimize the effect of scattering via optimizing the filtered tomographic back projections have already been successfully implemented<sup>34,43</sup>.

### Improving speed and resolution

The various vat-polymerization techniques feature different bioprinting speeds. In tomographic bioprinting, the time needed for production does not necessarily scale with the volume, making this technique the fastest. In DLP, the bioprinting speed is linearly related to the thickness of the construct, and for SLA and TPL, speed scales with the volume. Despite these differences, there are generally methods to improve the bioprinting speed of each modality. In DLP, for example, the continuous liquid interface approach enables fast creation of volumetric structures<sup>46,143,191,211</sup> by building an oxygen-containing dead zone into the bottom of the vat separating the patterned layers from the vat surface. The speed of the DLP process may be further enhanced by embedding a bioresin-immiscible fluid layer as the dead layer, which is further circulated to dissipate heat generated from photopolymerization<sup>212</sup>. For SLA, speed is aided by the light-sheet system<sup>213</sup>. A multifocus process that simultaneously generates and controls up to 10 laser foci further enables parallel nanofabrication through TPL<sup>214</sup>; alternatively, multiple beams can be used to also expedite the TPL procedure<sup>215</sup>.

Resolution is inversely proportional to the operational speed for the printing modalities. TPL has the highest resolution (tens of nanometre range) followed by SLA, DLP and VAM bioprinting techniques (micrometres to tens of micrometres). Resolution scales can vary depending on the specific setups. Some broad strategies for resolution enhancement include the utilization of 8K/16K DMD or other projection systems as the light-pattern sources. Other methods that can increase resolution include the synergy of two light sources, in which one photopolymerizes and the other inhibits polymerization<sup>44</sup>, volume shrinkage post-bioprinting<sup>216–218</sup> and the integration of feedback and correction algorithms into the software<sup>146,219</sup>.

### Outlook

In the past decade, light-based vat-polymerization bioprinting has gained traction within the fields of bioprinting and tissue engineering. The adoption of light-based vat-polymerization bioprinting is evidenced in multiple commercial systems recently coming to market<sup>5</sup>. There are several exciting emerging use cases as well as technological developments that, if validated, will enhance the performance and scope of light-based vat-polymerization bioprinting as a powerful tool for both life science research and clinical applications.

We are excited about early work in intelligent bioprinting by integrating machine learning with light-based bioprinting. One of the limiting factors of the spatial resolution of light-based polymerization, which is only exacerbated in cell-laden bioprinting, is the effect of light scattering<sup>220</sup>. The effect of light scattering on resolution can be reduced to an extent by trial-and-error modification of the printing parameters and printing solution composition (by adding photoabsorbers, for example); however, this is a tedious, time-intensive process and likely not to result in optimal resolution for fine features. Recently, machine learning using deep neural networks has been shown to be capable of generating digital masks with a modified geometry and greyscale values to produce a 3D-printed part of a preset specification with superior microscale resolution when compared with trial-and-error optimization<sup>221,222</sup>. Machine-learning optimization of the key properties of a bioprinted device or tissue – such as the resolution and mechanical properties – will eventually enable the specification of desired properties of a bioprinted construct for any given arbitrary geometry and known printing solution composition. A recent report showed a contrast-based focusing mechanism that could be automated for consistent single-digit microscale<sup>223</sup>. Automated focusing coupled with machine-learning optimization will eventually enable a non-expert user to simply input their 3D image file and desired mechanical properties, and the bioprinting system will do the rest.

There are currently no bioprinting solutions used in the clinic as the commercial use of the technology is in the nascent stage. The US Food and Drug Administration (FDA) has only just begun in the last year to consider developing regulatory guidance on using 3D printing technology in the clinical setting<sup>224</sup>. Light-based 3D printing is already widely adopted by the dentistry field, in which practitioners use 3D scanners with 3D printers to fabricate a myriad of patient-specific solutions ranging from crowns to surgical implants to mouthguards and retainers<sup>225,226</sup>. The FDA has not produced guidance on combining human cells or tissue with 3D-printed constructs in the clinic, let alone bioprinting. Light-based bioprinting has the greatest potential of the bioprinting modalities to be incorporated in the clinical setting as it has the quickest production process, does not induce mechanical stress on the cells and is capable of providing the highest resolution. Owing to the complexity in optimization and need for consistent microscale resolution to match injury-specific build specifications, automating the bioprinting process will be a necessary leap to integrate it into the clinical setting. Additionally, clinicians will need to be able to readily develop a bioprinted scaffold therapy based on the defect of a patient upon presentation. Already researchers have shown that they can transform 3D medical images into structures that match the geometric shape of a defect site<sup>200</sup>. To achieve bioprinting at the point-of-care, a turnkey ecosystem will have to be developed for a clinician to fabricate a patient-specific bioprinted scaffold directly from a 3D medical image of a defect site. Alternatively, intravital bioprinting (bioprinting directly at the site of injury or defect) has been reported using light-based vat-polymerization techniques<sup>175,202</sup>.

Published online: 22 June 2023

## References

- Groll, J. et al. Biofabrication: reappraising the definition of an evolving field. *Biofabrication* **8**, 013001 (2016).
- Levato, R. et al. From shape to function: the next step in bioprinting. *Adv. Mater.* **32**, 1906423 (2020).
- Moroni, L. et al. Biofabrication: a guide to technology and terminology. *Trends Biotechnol.* **36**, 384–402 (2018).
- Moroni, L. et al. Biofabrication strategies for 3D in vitro models and regenerative medicine. *Nat. Rev. Mater.* **3**, 21–37 (2018).
- Heinrich, M. A. et al. 3D bioprinting: from benches to translational applications. *Small* **15**, 1805510 (2019).
- Garciamendez-Mijares, C. E., Agrawal, P., García Martínez, G., Cervantes Juarez, E. & Zhang, Y. S. State-of-art affordable bioprinters: a guide for the DIY community. *Appl. Phys. Rev.* **8**, 031312 (2021).
- Hull, C. W. Apparatus for production of three-dimensional objects by stereolithography. US patent US4575330A (1986).
- Lu, Y. & Chen, S. C. Micro and nano-fabrication of biodegradable polymers for drug delivery. *Adv. Drug Del. Rev.* **56**, 1621–1633 (2004).
- Mapili, G., Lu, Y., Chen, S. & Roy, K. Laser-layered microfabrication of spatially patterned functionalized tissue-engineering scaffolds. *J. Biomed. Mater. Res. A* **75**, 414–424 (2005).
- Dharwala, B., Hunt, E. & Boland, T. Rapid prototyping of tissue-engineering constructs, using photopolymerizable hydrogels and stereolithography. *Tissue Eng.* **10**, 1316–1322 (2004).
- Li, W. et al. Stereolithography apparatus and digital light processing-based 3D bioprinting for tissue fabrication. *iScience* **26**, 106039 (2023).
- Yu, C. et al. Photopolymerizable biomaterials and light-based 3D printing strategies for biomedical applications. *Chem. Rev.* **120**, 10695–10743 (2020).
- Zuev, D. M., Nguyen, A. K., Putlyaev, V. I. & Narayan, R. J. 3D printing and bioprinting using multiphoton lithography. *Bioprinting* **20**, e00090 (2020).
- Zandirini, T., Florczak, S., Levato, R. & Ovsianikov, A. Breaking the resolution limits of 3D bioprinting: future opportunities and present challenges. *Trends Biotechnol.* **41**, 604–614 (2022).
- Shusteff, M. et al. One-step volumetric additive manufacturing of complex polymer structures. *Sci. Adv.* **3**, eaao5496 (2017).
- Regehly, M. et al. Xolography for linear volumetric 3D printing. *Nature* **588**, 620–624 (2020).
- Ruskowitz, E. R. & Deforest, C. A. Photoresponsive biomaterials for targeted drug delivery and 4D cell culture. *Nat. Rev. Mater.* **3**, 17087 (2018).
- Zhang, Y. S. et al. 3D extrusion bioprinting. *Nat. Rev. Methods Primers* **1**, 75 (2021).
- Guillemot, F., Mironov, V. & Nakamura, M. Bioprinting is coming of age: report from the international conference on bioprinting and biofabrication in bordeaux (3B'09). *Biofabrication* **2**, 010201 (2010).
- Groll, J. et al. A definition of bioinks and their distinction from biomaterial inks. *Biofabrication* **11**, 013001 (2018).
- Zhou, X., Hou, Y. & Lin, J. A review on the processing accuracy of two-photon polymerization. *AIP Adv.* **5**, 030701 (2015).
- Lee, M., Rizzo, R., Surman, F. & Zenobi-Wong, M. Guiding lights: tissue bioprinting using photoactivated materials. *Chem. Rev.* **120**, 10950–11027 (2020).
- Harinrayana, V. & Shin, Y. C. Two-photon lithography for three-dimensional fabrication in micro/nanoscale regime: a comprehensive review. *Opt. Laser Technol.* **142**, 107180 (2021).
- Skoog, S. A., Goering, P. L. & Narayan, R. J. Stereolithography in tissue engineering. *J. Mater. Sci. Mater. Med.* **25**, 845–856 (2014).
- Kuo, A. P. et al. High-precision stereolithography of biomicrofluidic devices. *Adv. Mater. Technol.* **4**, 1800395 (2019).
- Li, H. et al. Digital light processing (DLP)-based (bio)printing strategies for tissue modeling and regeneration. *Aggregate* **4**, e270 (2022).
- Kowsari, K., Lee, W., Yoo, S.-S. & Fang, N. X. Scalable visible light 3D printing and bioprinting using an organic light-emitting diode microdisplay. *iScience* **24**, 103372 (2021).
- Hosseiniabadi, H. G. et al. Ink material selection and optical design considerations in DLP 3D printing. *Appl. Mater. Today* **30**, 101721 (2023).
- Lu, Y., Mapili, G., Suhali, G., Chen, S. & Roy, K. A digital micro-mirror device-based system for the microfabrication of complex, spatially patterned tissue engineering scaffolds. *J. Biomed. Mater. Res. A* **77**, 396–405 (2006).
- Ma, X. et al. Deterministically patterned biomimetic human iPSC-derived hepatic model via rapid 3D bioprinting. *Proc. Natl. Acad. Sci. USA* **113**, 2206–2211 (2016).
- Gauvin, R. et al. Microfabrication of complex porous tissue engineering scaffolds using 3D projection stereolithography. *Biomaterials* **33**, 3824–3834 (2012).
- Kelly, B. E. et al. Volumetric additive manufacturing via tomographic reconstruction. *Science* **363**, 1075–1079 (2019).
- Bernal, P. N. et al. Volumetric bioprinting of complex living-tissue constructs within seconds. *Adv. Mater.* **31**, 1904209 (2019).
- Bernal, P. N. et al. Volumetric bioprinting of organoids and optically tuned hydrogels to build liver-like metabolic biofactories. *Adv. Mater.* **34**, 2110054 (2022).
- Toombs, J. T. et al. Volumetric additive manufacturing of silica glass with microscale computed axial lithography. *Science* **376**, 308–312 (2022).
- Li, W. et al. Recent advances in formulating and processing biomaterial inks for vat polymerization-based 3D printing. *Adv. Healthc. Mater.* **9**, 2000156 (2020).
- Murphy, C. A., Lim, K. S. & Woodfield, T. B. F. Next evolution in organ-scale biofabrication: bioresin design for rapid high-resolution vat polymerization. *Adv. Mater.* **34**, 2107759 (2022).
- Bader, C. et al. Making data matter: voxel printing for the digital fabrication of data across scales and domains. *Sci. Adv.* **4**, eaas8652 (2018).
- Hiller, J. & Lipson, H. Design and analysis of digital materials for physical 3D voxel printing. *Rapid Prototyp. J.* **15**, 137–149 (2009).
- Wu, C., Yi, R., Liu, Y. J., He, Y. & Wang, C. C. L. in 2016 IEEE/RSJ International Conference on Intelligent Robots and Systems (IROS) 2155–2160 (IEEE, 2016).
- Huang, J., Ware, H. O. T., Hai, R., Shao, G. & Sun, C. Conformal geometry and multimaterial additive manufacturing through freeform transformation of building layers. *Adv. Mater.* **33**, 2005672 (2021).

42. Kwok, T.-H. Comparing slicing technologies for digital light processing printing. *J. Comput. Inf. Sci. Eng.* **19**, 044502 (2019).
43. Madrid-Wolf, J., Boniface, A., Loterie, D., Delrot, P. & Moser, C. Controlling light in scattering materials for volumetric additive manufacturing. *Adv. Sci.* **9**, 2105144 (2022).
44. De Beer, M. P. et al. Rapid, continuous additive manufacturing by volumetric polymerization inhibition patterning. *Sci. Adv.* **5**, eaau8723 (2019).
45. Lipkowitz, G. et al. Injection continuous liquid interface production of 3D objects. *Sci. Adv.* **8**, eabq3917 (2022).
46. Tumbleston, J. R. et al. Continuous liquid interface production of 3D objects. *Science* **347**, 1349 (2015).
47. Wang, B. et al. Stiffness control in dual color tomographic volumetric 3D printing. *Nat. Commun.* **13**, 367 (2022).
48. Sameni, F. et al. Hot lithography vat photopolymerisation 3D printing: vat temperature vs. mixture design. *Polymers* **14**, 2988 (2022).
49. Morgan, F. L. C., Moroni, L. & Baker, M. B. Dynamic bioinks to advance bioprinting. *Adv. Healthc. Mater.* **9**, e1901798 (2020).
50. Dong, Y. et al. Engineering the cell microenvironment using novel photoresponsive hydrogels. *ACS Appl. Mater. Interfaces* **10**, 12374–12389 (2018).
51. Adhikari, J. et al. Effects of processing parameters of 3D bioprinting on the cellular activity of bioinks. *Macromol. Biosci.* **21**, e2000179 (2021).
52. Ng, W. L. et al. Vat polymerization-based bioprinting-process, materials, applications and regulatory challenges. *Biofabrication* **12**, 022001 (2020).
53. Shadish, J. A., Benuska, G. M. & Deforest, C. A. Bioactive site-specifically modified proteins for 4D patterning of gel biomaterials. *Nat. Mater.* **18**, 1005–1014 (2019).
54. Wang, M. et al. Digital light processing-based bioprinting with composable gradients. *Adv. Mater.* **34**, 2107038 (2022).
55. Yu, C. et al. A sequential 3D bioprinting and orthogonal bioconjugation approach for precision tissue engineering. *Biomaterials* **258**, 120294 (2020).
56. Ravanbakhsh, H., Bao, G., Luo, Z., Mongeau, L. G. & Zhang, Y. S. Composite Inks for extrusion printing of biological and biomedical constructs. *ACS Biomater. Sci. Eng.* **7**, 4009–4026 (2021).
57. Zhang, S. et al. Convergence of 3D bioprinting and nanotechnology in tissue engineering scaffolds. *Biomimetics* **8**, 94 (2023).
58. Loukels, K., Helal, Z. A., Mikos, A. G. & Chatzinkalaidou, M. Nanocomposite bioprinting for tissue engineering applications. *Gels* **9**, 103 (2023).
59. Alcala-Orozco, C. R. et al. Design and characterisation of multi-functional strontium-gelatin nanocomposite bioinks with improved print fidelity and osteogenic capacity. *Bioprinting* **18**, e00073 (2020).
60. Li, L. et al. Methacrylate-modified gold nanoparticles enable noninvasive monitoring of photocrosslinked hydrogel scaffolds. *Adv. NanoBiomed Res.* **2**, 2200022 (2022).
61. Tao, J. et al. Nanoparticle-stabilized emulsion bioink for digital light processing based 3D bioprinting of porous tissue constructs. *Adv. Healthc. Mater.* **11**, 2102810 (2022).
62. Ouyang, L., Wojciechowski, J. P., Tang, J., Guo, Y. & Stevens, M. M. Tunable microgel-templated porogel (MTP) bioink for 3D bioprinting applications. *Adv. Healthc. Mater.* **11**, 2200027 (2022).
63. Ying, G.-L. et al. Aqueous two-phase emulsion bioink-enabled 3D bioprinting of porous hydrogels. *Adv. Mater.* **30**, 1805460 (2018).
64. Yi, S. et al. Micropore-forming gelatin methacryloyl (GelMA) bioink toolbox 2.0: designable tunability and adaptability for 3D bioprinting applications. *Small* **18**, 2106357 (2022).
65. Lim, K. S. et al. Fundamentals and applications of photo-cross-linking in bioprinting. *Chem. Rev.* **120**, 10662–10694 (2020).
66. Tomal, W. & Ortyl, J. Water-soluble photoinitiators in biomedical applications. *Polymers* **12**, 1073 (2020).
67. Lim, K. S. et al. Visible light cross-linking of gelatin hydrogels offers an enhanced cell microenvironment with improved light penetration depth. *Macromol. Biosci.* **19**, 1900098 (2019).
68. Wu, Y., Simpson, M. C. & Jin, J. Fast hydrolytically degradable 3D printed object based on aliphatic polycarbonate thiol-ene photoresins. *Macromol. Chem. Phys.* **222**, 20000435 (2021).
69. Tibbitt, M. W., Kloxin, A. M., Sawicki, L. & Anseth, K. S. Mechanical properties and degradation of chain and step polymerized photodegradable hydrogels. *Macromolecules* **46**, 2785–2792 (2013).
70. Scinto, S. L. et al. Bioorthogonal chemistry. *Nat. Rev. Methods Primers* **1**, 30 (2021).
71. Fairbanks, B. D. et al. Photoclick chemistry: a bright idea. *Chem. Rev.* **121**, 6915–6990 (2021).
72. Albada, B., Keijzer, J. F., Zuilhof, H. & Van Delft, F. Oxidation-induced ‘one-pot’ click chemistry. *Chem. Rev.* **121**, 7032–7058 (2021).
73. Kim, H. et al. Light-activated decellularized extracellular matrix-based bioinks for volumetric tissue analogs at the centimeter scale. *Adv. Funct. Mater.* **31**, 2011252 (2021).
74. Bjork, J. W., Johnson, S. L. & Tranquillo, R. T. Ruthenium-catalyzed photo cross-linking of fibrin-based engineered tissue. *Biomaterials* **32**, 2479–2488 (2011).
75. Lim, K. S. et al. New visible-light photoinitiatting system for improved print fidelity in gelatin-based bioinks. *ACS Biomater. Sci. Eng.* **2**, 1752–1762 (2016).
76. Soltman, B. G. et al. Programming delayed dissolution into sacrificial bioinks for dynamic temporal control of architecture within 3D-bioprinted constructs. *Adv. Funct. Mater.* **33**, 2210521 (2023).
77. Xie, M. et al. Volumetric additive manufacturing of pristine silk-based (bio)inks. *Nat. Commun.* **14**, 210 (2023).
78. Rydholm, A. E., Bowman, C. N. & Anseth, K. S. Degradable thiol-acrylate photopolymers: polymerization and degradation behavior of an *in situ* forming biomaterial. *Biomaterials* **26**, 4495–4506 (2005).
79. Haris, U., Plank, J. T., Li, B., Page, Z. A. & Lippert, A. R. Visible light chemical micropatterning using a digital light processing fluorescence microscope. *ACS Cent. Sci.* **8**, 67–76 (2022).
80. Rizzo, R., Ruetsche, D., Liu, H. & Zenobi-Wong, M. Optimized photoclick (bio)resins for fast volumetric bioprinting. *Adv. Mater.* **33**, 2102900 (2021).
81. Bertassoni, L. E. Bioprinting of complex multicellular organs with advanced functionality—recent progress and challenges ahead. *Adv. Mater.* **34**, e2101321 (2022).
82. Dhand, A. P. et al. Simultaneous one-pot interpenetrating network formation to expand 3D processing capabilities. *Adv. Mater.* **34**, e2202261 (2022).
83. Caprioli, M. et al. 3D-printed self-healing hydrogels via digital light processing. *Nat. Commun.* **12**, 2462 (2021).
84. Schwab, A. et al. Printability and shape fidelity of bioinks in 3D bioprinting. *Chem. Rev.* **120**, 11028–11055 (2020).
85. Durand-Silva, A. et al. Balancing self-healing and shape stability in dynamic covalent photoresins for stereolithography 3D printing. *ACS Macro Lett.* **10**, 486–491 (2021).
86. Robinson, L. L. et al. Chemical and mechanical tunability of 3D-printed dynamic covalent networks based on boronate esters. *ACS Macro Lett.* **10**, 857–863 (2021).
87. Wilts, E. M. et al. Vat photopolymerization of charged monomers: 3D printing with supramolecular interactions. *Polym. Chem.* **10**, 1442–1451 (2019).
88. Uzcategui, A. C., Muralidharan, A., Ferguson, V. L., Bryant, S. J. & Mcleod, R. R. Understanding and improving mechanical properties in 3D printed parts using a dual-cure acrylate-based resin for stereolithography. *Adv. Eng. Mater.* **20**, 1800876 (2018).
89. Stevens, L. M., Tagnon, C. & Page, Z. A. ‘Invisible’ digital light processing 3D printing with near infrared light. *ACS Appl. Mater. Interfaces* **14**, 22912–22920 (2022).
90. Sanders, S. N. et al. Triplet fusion upconversion nanocapsules for volumetric 3D printing. *Nature* **604**, 474–478 (2022).
91. Thijssen, Q. et al. Volumetric printing of thiol-ene photo-cross-linkable poly(ε-caprolactone): a tunable material platform serving biomedical applications. *Adv. Mater.* <https://doi.org/10.1002/adma.202210136> (2023).
92. Hahn, V. et al. Two-step absorption instead of two-photon absorption in 3D nanoprinting. *Nat. Photon.* **15**, 932–938 (2021).
93. Hahn, V. et al. Light-sheet 3D microprinting via two-colour two-step absorption. *Nat. Photon.* **16**, 784–791 (2022).
94. Mensov, S. N. et al. Use of photodegradable inhibitors in UV-curable compositions to form polymeric 2D-structures by visible light. *J. Appl. Polym. Sci.* **137**, 48976 (2020).
95. Goodarzi Hosseiniabadi, H., Dogan, E., Miri, A. K. & Ionov, L. Digital light processing bioprinting advances for microtissue models. *ACS Biomater. Sci. Eng.* **8**, 1381–1395 (2022).
96. You, S. et al. High cell density and high resolution 3D bioprinting for fabricating vascularized tissues. *Sci. Adv.* **9**, eade7923 (2023).
97. Rizzo, R., Petelinšek, N., Bonato, A. & Zenobi-Wong, M. From free-radical to radical-free: a paradigm shift in light-mediated biofabrication. *Adv. Sci.* **10**, e2205302 (2023).
98. Bao, Y., Paunovic, N. & Leroux, J. C. Challenges and opportunities in 3D printing of biodegradable medical devices by emerging photopolymerization techniques. *Adv. Funct. Mater.* **32**, 2109864 (2022).
99. Beh, C. W. et al. A fluid-supported 3D hydrogel bioprinting method. *Biomaterials* **276**, 121034 (2021).
100. Brown, T. E. et al. Voxel-scale conversion mapping informs intrinsic resolution in stereolithographic additive manufacturing. *ACS Appl. Polym. Mater.* **3**, 290–298 (2020).
101. Salvekar, A. V. et al. Rapid volumetric additive manufacturing in solid state: a demonstration to produce water-content-dependent cooling/heating/water-responsive shape memory hydrogels. *3D Print. Add. Manuf.* <https://doi.org/10.1089/3dp.2021.0279> (2022).
102. Kloxin, A. M., Kasko, A. M., Salinas, C. N. & Anseth, K. S. Photodegradable hydrogels for dynamic tuning of physical and chemical properties. *Science* **324**, 59–63 (2009).
103. McKinnon, D. D., Brown, T. E., Kyburz, K. A., Kiyotake, E. & Anseth, K. S. Design and characterization of a synthetically accessible, photodegradable hydrogel for user-directed formation of neural networks. *Biomacromolecules* **15**, 2808–2816 (2014).
104. Xie, R., Zheng, W., Guan, L., Ai, Y. & Liang, Q. Engineering of hydrogel materials with perfusable microchannels for building vascularized tissues. *Small* **16**, e1902838 (2020).
105. Brown, T. E., Marozas, I. A. & Anseth, K. S. Amplified photodegradation of cell-laden hydrogels via an addition-fragmentation chain transfer reaction. *Adv. Mater.* **29**, 1605001 (2017).
106. Nelson, B. R. et al. Photoinduced dithiolane crosslinking for multiresponsive dynamic hydrogels. *Adv. Mater.* <https://doi.org/10.1002/adma.202211209> (2023).
107. Tavafoghi, M. et al. Multimaterial bioprinting and combination of processing techniques towards the fabrication of biomimetic tissues and organs. *Biofabrication* <https://doi.org/10.1088/1758-5090/ac0b9a> (2021).
108. Davidson, M. D. et al. Programmable and contractile materials through cell encapsulation in fibrous hydrogel assemblies. *Sci. Adv.* **7**, eabi8157 (2021).

109. Carrberry, B. J. et al. 3D printing of sacrificial thioester elastomers using digital light processing for templating 3D organoid structures in soft biomatrices. *Biofabrication* **13**, 044104 (2021).
110. Wang, M. et al. Molecularly cleavable bioinks facilitate high-performance digital light processing-based bioprinting of functional volumetric soft tissues. *Nat. Commun.* **13**, 3317 (2022).
111. Levato, R. et al. High-resolution lithographic biofabrication of hydrogels with complex microchannels from low-temperature-soluble gelatin bioresins. *Mater. Today Bio* **12**, 100162 (2021).
112. Müller, M. Z., Style, R. W., Müller, R. & Qin, X.-H. A phase-separating thiol-ene photoresin for volumetric bioprinting of macroporous hydrogels. Preprint at *bioRxiv* <https://doi.org/10.1101/2022.01.29.478338> (2022).
113. Qin, X.-S., Wang, M., Li, W. & Zhang, Y. S. Biosurfactant-stabilized micropore-forming GelMA Inks enable improved usability for 3D printing applications. *Regen. Eng. Transl. Med.* **8**, 471–481 (2022).
114. Sampson, K. L. et al. Multimaterial vat polymerization additive manufacturing. *ACS Appl. Polym. Mater.* **3**, 4304–4324 (2021).
115. Ravangbakhsh, H. et al. Emerging technologies in multi-material bioprinting. *Adv. Mater.* **33**, 2104730 (2021).
116. Choi, J.-W., Kim, H.-C. & Wicker, R. Multi-material stereolithography. *J. Mater. Process. Technol.* **211**, 318–328 (2011).
117. Grigoryan, B. et al. Development, characterization, and applications of multi-material stereolithography bioprinting. *Sci. Rep.* **11**, 3171 (2021).
118. Liao, J. et al. 3D-printable colloidal photonic crystals. *Mater. Today* **56**, 29–41 (2022).
119. Cheng, J. et al. Centrifugal multimaterial 3D printing of multifunctional heterogeneous objects. *Nat. Commun.* **13**, 7931 (2022).
120. Miri, A. K. et al. Microfluidics-enabled multimaterial maskless stereolithographic bioprinting. *Adv. Mater.* **30**, 1800242 (2018).
121. Han, D., Yang, C., Fang, N. X. & Lee, H. Rapid multi-material 3D printing with projection micro-stereolithography using dynamic fluidic control. *Add. Manuf.* **27**, 606–615 (2019).
122. Liu, J., Hwang, H. H., Wang, P., Whang, G. & Chen, S. Direct 3D-printing of cell-laden constructs in microfluidic architectures. *Lab Chip* **16**, 1430–1438 (2016).
123. Chansoria, P. et al. Synergizing algorithmic design, photoclick chemistry and multi-material volumetric printing for accelerating complex shape engineering. Preprint at *bioRxiv* <https://doi.org/10.1101/2022.11.29.518318> (2022).
124. Bialas, S. et al. Access to disparate soft matter materials by curing with two colors of light. *Adv. Mater.* **31**, 1807288 (2019).
125. Schwartz, J. J. & Boydston, A. J. Multimaterial actinic spatial control 3D and 4D printing. *Nat. Commun.* **10**, 791 (2019).
126. Peng, X. et al. Multi-color 3D printing via single-vat grayscale digital light processing. *Adv. Funct. Mater.* **32**, 2112329 (2022).
127. Kuang, X. et al. Grayscale digital light processing 3D printing for highly functionally graded materials. *Sci. Adv.* **5**, eaav5790 (2019).
128. Yue, L. et al. Single-vat single-cure grayscale digital light processing 3D printing of materials with large property difference and high stretchability. *Nat. Commun.* **14**, 1251 (2023).
129. Shanjani, Y., Pan, C. C., Elomaa, L. & Yang, Y. A novel bioprinting method and system for forming hybrid tissue engineering constructs. *Biofabrication* **7**, 045008 (2015).
130. An, H. S. et al. High-resolution 3D printing of freeform, transparent displays in ambient air. *Adv. Sci.* **6**, 1901603 (2019).
131. Greenhall, J. & Raeymaekers, B. 3D printing macroscale engineered materials using ultrasound directed self-assembly and stereolithography. *Adv. Mater. Technol.* **2**, 1700122 (2017).
132. Lu, L., Tang, X., Hu, S. & Pan, Y. Acoustic field-assisted particle patterning for smart polymer composite fabrication in stereolithography. *3D Print. Add. Manuf.* **5**, 151–159 (2018).
133. Wang, Y. et al. Acoustic-assisted 3D printing based on acoustofluidic microparticles patterning for conductive polymer composites fabrication. *Add. Manuf.* **60**, 103247 (2022).
134. Kunwar, P. et al. Hybrid laser printing of 3D, multiscale, multimaterial hydrogel structures. *Adv. Opt. Mater.* **7**, 1900656 (2019).
135. Rizzo, R. et al. Multiscale hybrid fabrication: volumetric printing meets two-photon ablation. Preprint at *bioRxiv* <https://doi.org/10.1101/202201871> (2022).
136. Größbacher, G. et al. Volumetric printing across melt electrowritten scaffolds fabricates multi-material living constructs with tunable architecture and mechanics. *Adv. Mater.* <https://doi.org/10.1002/adma.202300756> (2023).
137. Huh, J. et al. Combinations of photoinitiator and UV absorber for cell-based digital light processing (DLP) bioprinting. *Biofabrication* **13**, 034103 (2021).
138. Bennett, J. Measuring UV curing parameters of commercial photopolymers used in additive manufacturing. *Add. Manuf.* **18**, 203–212 (2017).
139. Seck, T. M., Melchels, F. P. W., Feijen, J. & Grijpma, D. W. Designed biodegradable hydrogel structures prepared by stereolithography using poly(ethylene glycol)/poly(D,L-lactide)-based resins. *J. Control. Rel.* **148**, 34–41 (2010).
140. Van Hoorick, J. et al. Cross-linkable gelatins with superior mechanical properties through carboxylic acid modification: increasing the two-photon polymerization potential. *Biomacromolecules* **18**, 3260–3272 (2017).
141. Galarraga, J. H., Dhand, A. P., Enzmann, B. P., Iii & Burdick, J. A. Synthesis, characterization, and digital light processing of a hydrolytically degradable hyaluronic acid hydrogel. *Biomacromolecules* **24**, 413–425 (2023).
142. Sanchez Noriega, J. L. et al. Spatially and optically tailored 3D printing for highly miniaturized and integrated microfluidics. *Nat. Commun.* **12**, 5509 (2021).
143. Grigoryan, B. et al. Multivasular networks and functional intravascular topologies within biocompatible hydrogels. *Science* **364**, 458 (2019).
144. Khoon, S. L. et al. Bio-resin for high resolution lithography-based biofabrication of complex cell-laden constructs. *Biofabrication* **10**, 034101 (2018).
145. Janusziewicz, R., Tumbleston, J. R., Quintanilla, A. L., Mecham, S. J. & Desimone, J. M. Layerless fabrication with continuous liquid interface production. *Proc. Natl Acad. Sci. USA* **113**, 11703–11708 (2016).
146. Loterie, D., Delrot, P. & Moser, C. High-resolution tomographic volumetric additive manufacturing. *Nat. Commun.* **11**, 852 (2020).
147. Salajeghe, R., Meile, D. H., Kruse, C. S., Marla, D. & Spangenberg, J. Numerical modeling of part sedimentation during volumetric additive manufacturing. *Addit. Manuf.* **66**, 103459 (2022).
148. Caliari, S. R. & Burdick, J. A. A practical guide to hydrogels for cell culture. *Nat. Methods* **13**, 405–414 (2016).
149. Fedorovich, N. E. et al. The effect of photopolymerization on stem cells embedded in hydrogels. *Biomaterials* **30**, 344–353 (2009).
150. Ruskowitz, E. R. & Deforest, C. A. Proteome-wide analysis of cellular response to ultraviolet light for biomaterial synthesis and modification. *ACS Biomater. Sci. Eng.* **5**, 2111–2116 (2019).
151. Bartnikowski, M., Bartnikowski, N. J., Woodruff, M. A., Schrobback, K. & Klein, T. J. Protective effects of reactive functional groups on chondrocytes in photocrosslinkable hydrogel systems. *Acta Biomater.* **27**, 66–76 (2015).
152. Kratochvíl, M. J. et al. Engineered materials for organoid systems. *Nat. Rev. Mater.* **4**, 606–622 (2019).
153. Ovsianikov, A., Mironov, V., Stampfli, J. & Liska, R. Engineering 3D cell-culture matrices: multiphoton processing technologies for biological and tissue engineering applications. *Exp. Rev. Med. Device* **9**, 613–633 (2012).
154. Dobos, A. et al. On-chip high-definition bioprinting of microvascular structures. *Biofabrication* **13**, 015016 (2021).
155. Marino, A. et al. The Osteoprint: a bioinspired two-photon polymerized 3-D structure for the enhancement of bone-like cell differentiation. *Acta Biomater.* **10**, 4304–4313 (2014).
156. Marino, A. et al. A 3D real-scale, biomimetic, and biohybrid model of the blood-brain barrier fabricated through two-photon lithography. *Small* **14**, 1702959 (2018).
157. Krüger, H., Asido, M., Wachtweit, J., Tampé, R. & Wieneke, R. Sensitizer-enhanced two-photon patterning of biomolecules in photoinsensitive hydrogels. *Commun. Mater.* **3**, 9 (2022).
158. Broguiere, N. et al. Morphogenesis guided by 3D patterning of growth factors in biological matrices. *Adv. Mater.* **32**, 1908299 (2020).
159. Qin, X.-H., Wang, X., Rottmar, M., Nelson, B. J. & Maniura-Weber, K. Near-infrared light-sensitive polyvinyl alcohol hydrogel photoresist for spatiotemporal control of cell-instructive 3D microenvironments. *Adv. Mater.* **30**, 1705564 (2018).
160. Skylar-Scott, M. A., Liu, M. C., Wu, Y., Dixit, A. & Yanik, M. F. Guided homing of cells in multi-photon microfabricated bioscaffolds. *Adv. Healthc. Mater.* **5**, 1233–1243 (2016).
161. Deforest, C. A. & Anseth, K. S. Cytocompatible click-based hydrogels with dynamically tunable properties through orthogonal photoconjugation and photocleavage reactions. *Nat. Chem.* **3**, 925–931 (2011).
162. Arakawa, C. K., Badeau, B. A., Zheng, Y. & Deforest, C. A. Multicellular vascularized engineered tissues through user-programmable biomaterial photodegradation. *Adv. Mater.* **29**, 1703156 (2017).
163. Rayner, S. G. et al. Multiphoton-guided creation of complex organ-specific microvasculature. *Adv. Healthc. Mater.* **10**, 2100031 (2021).
164. Enrico, A. et al. 3D microvascularized tissue models by laser-based cavitation molding of collagen. *Adv. Mater.* **34**, 2109823 (2022).
165. Ovsianikov, A. et al. Laser photofabrication of cell-containing hydrogel constructs. *Langmuir* **30**, 3787–3794 (2014).
166. Tromayer, M. et al. A biocompatible macromolecular two-photon initiator based on hyaluronan. *Polym. Chem.* **8**, 451–460 (2017).
167. Tromayer, M. et al. A biocompatible diazosulfonate initiator for direct encapsulation of human stem cells via two-photon polymerization. *Polym. Chem.* **9**, 3108–3117 (2018).
168. Lee, S. et al. A needle-type microrobot for targeted drug delivery by affixing to a microtissue. *Adv. Healthc. Mater.* **9**, 1901697 (2020).
169. Cabanach, P. et al. Zwitterionic 3D-printed non-immunogenic stealth microrobots. *Adv. Mater.* **32**, 2003013 (2020).
170. Ceylan, H. et al. 3D-printed biodegradable microswimmer for theranostic cargo delivery and release. *ACS Nano* **13**, 3353–3362 (2019).
171. Yasa, I. C., Tabak, A. F., Yasa, O., Ceylan, H. & Sitti, M. 3D-printed microrobotic transporters with recapitulated stem cell niche for programmable and active cell delivery. *Adv. Funct. Mater.* **29**, 1808992 (2019).
172. Cordeiro, A. S. et al. Two-photon polymerization 3D printing of microneedle array templates with versatile designs: application in the development of polymeric drug delivery systems. *Pharmac. Res.* **37**, 174 (2020).
173. Lemma, E. D., Spagnolo, B., De Vittorio, M. & Pisanello, F. Studying cell mechanobiology in 3D: the two-photon lithography approach. *Trends Biotechnol.* **37**, 358–372 (2019).

174. Tibbitt, M. W., Kloxin, A. M., Dyamnehalli, K. U. & Anseth, K. S. Controlled two-photon photodegradation of PEG hydrogels to study and manipulate subcellular interactions on soft materials. *Soft Matter* **6**, 5100–5108 (2010).
175. Urciuolo, A. et al. Intravital three-dimensional bioprinting. *Nat. Biomed. Eng.* **4**, 901–915 (2020).
176. Abele, T. et al. Two-photon 3D laser printing inside synthetic cells. *Adv. Mater.* **34**, 2106709 (2022).
177. Zhong, Z. et al. Rapid 3D bioprinting of a multicellular model recapitulating pterygium microenvironment. *Biomaterials* **282**, 121391 (2022).
178. Soliman, B. G. et al. Development and characterization of gelatin-norbornene bioink to understand the interplay between physical architecture and micro-capillary formation in biofabricated vascularized constructs. *Adv. Healthc. Mater.* **11**, 2101873 (2022).
179. Sun, A. X., Lin, H., Beck, A. M., Kilroy, E. J. & Tuan, R. S. Projection stereolithographic fabrication of human adipose stem cell-incorporated biodegradable scaffolds for cartilage tissue engineering. *Front. Bioeng. Biotechnol.* **3**, 115 (2015).
180. He, B. et al. 3D printed biomimetic epithelium/stroma bilayer hydrogel implant for corneal regeneration. *Bioact. Mater.* **17**, 234–247 (2022).
181. Elomaa, L. et al. Three-dimensional fabrication of cell-laden biodegradable poly(ethylene glycol-co-depsipeptide) hydrogels by visible light stereolithography. *J. Mater. Chem. B* **3**, 8348–8358 (2015).
182. Zhu, W. et al. Direct 3D bioprinting of vascularized tissue constructs with complex microarchitecture. *Biomaterials* **124**, 106–115 (2017).
183. Kiratitanaporn, W. et al. 3D printing a biocompatible elastomer for modeling muscle regeneration after volumetric muscle loss. *Biomater. Adv.* **142**, 213171 (2022).
184. Ma, X. et al. Rapid 3D bioprinting of decellularized extracellular matrix with regionally varied mechanical properties and biomimetic microarchitecture. *Biomaterials* **185**, 310–321 (2018).
185. Grix, T. et al. Bioprinting perfusion-enabled liver equivalents for advanced organ-on-a-chip applications. *Genes* **9**, 176 (2018).
186. Ma, Y. et al. Biomacromolecule-based agent for high-precision light-based 3D hydrogel bioprinting. *Cell Rep. Phys. Sci.* **3**, 100985 (2022).
187. Kim, S. H. et al. Precisely printable and biocompatible silk fibroin bioink for digital light processing 3D printing. *Nat. Commun.* **9**, 1620 (2018).
188. Tang, M. et al. Three-dimensional bioprinted glioblastoma microenvironments model cellular dependencies and immune interactions. *Cell Res.* **30**, 833–853 (2020).
189. Bracaglia, L. G. et al. 3D printed pericardium hydrogels to promote wound healing in vascular applications. *Biomacromolecules* **18**, 3802–3811 (2017).
190. 3D Systems. 3D systems announces breakthrough in bioprinting technology and expansion of regenerative medicine initiative. *3D Systems* <https://www.3dsystems.com/press-releases/3d-systems-announces-breakthrough-bioprinting-technology-and-expansion-0> (2021).
191. Anandakrishnan, N. et al. Fast stereolithography printing of large-scale biocompatible hydrogel models. *Adv. Healthc. Mater.* **10**, 2002103 (2021).
192. Shopperly, L. K. et al. Blends of gelatin and hyaluronic acid stratified by stereolithographic bioprinting approximate cartilaginous matrix gradients. *J. Biomed. Mater. Res. B* **110**, 2310–2322 (2022).
193. Xie, C. et al. High-efficient engineering of osteo-callus organoids for rapid bone regeneration within one month. *Biomaterials* **288**, 121741 (2022).
194. Yang, H. et al. Fabricating hydrogels to mimic biological tissues of complex shapes and high fatigue resistance. *Mater.* **4**, 1935–1946 (2021).
195. Wei, Y. et al. Stereolithography-based additive manufacturing of high-performance osteoinductive calcium phosphate ceramics by a digital light-processing system. *ACS Biomater. Sci. Eng.* **6**, 1787–1797 (2020).
196. Zhang, B. et al. Three-dimensional printing of large-scale, high-resolution bioceramics with micronano inner porosity and customized surface characterization design for bone regeneration. *ACS Appl. Mater. Interfaces* **14**, 8804–8815 (2022).
197. De Oliveira, M. F., Da Silva, L. C. E. & De Oliveira, M. G. 3D printed bioresorbable nitric oxide-releasing vascular stents. *Bioprinting* **22**, e00137 (2021).
198. Zhu, W. et al. Rapid continuous 3D printing of customizable peripheral nerve guidance conduits. *Mater. Today* **21**, 951–959 (2018).
199. Tao, J. et al. Rapid 3D printing of functional nanoparticle-enhanced conduits for effective nerve repair. *Acta Biomater.* **90**, 49–59 (2019).
200. Koffler, J. et al. Biomimetic 3D-printed scaffolds for spinal cord injury repair. *Nat. Med.* **25**, 263–269 (2019).
201. Liu, H. et al. Filamented light (FLight) biofabrication of highly aligned tissue-engineered constructs. *Adv. Mater.* **34**, 2204301 (2022).
202. Chen, Y. et al. Noninvasive in vivo 3D bioprinting. *Sci. Adv.* **6**, eaba7406 (2020).
203. Wang, Y. et al. 4D printed cardiac construct with aligned myofibers and adjustable curvature for myocardial regeneration. *ACS Appl. Mater. Interfaces* **13**, 12746–12758 (2021).
204. Dong, M. et al. Digital light processing 3D printing of tough supramolecular hydrogels with sophisticated architectures as impact-absorption elements. *Adv. Mater.* **34**, 2204333 (2022).
205. Xue, D., Zhang, J., Wang, Y. & Mei, D. Digital light processing-based 3D printing of cell-seeding hydrogel scaffolds with regionally varied stiffness. *ACS Biomater. Sci. Eng.* **5**, 4825–4833 (2019).
206. Gehlen, J., Qiu, W., Schädl, G. N., Müller, R. & Qin, X.-H. Tomographic volumetric bioprinting of heterocellular bone-like tissues in seconds. *Acta Biomater.* **156**, 49–60 (2022).
207. Wolf, K. J., Weiss, J. D., Uzel, S. G. M., Skylar-Scott, M. A. & Lewis, J. A. Biomanufacturing human tissues via organ building blocks. *Cell Stem Cell* **29**, 667–677 (2022).
208. Rackson, C. M. et al. Latent image volumetric additive manufacturing. *Opt. Lett.* **47**, 1279–1282 (2022).
209. Van Der Laan, H. L., Burns, M. A. & Scott, T. F. Volumetric photopolymerization confinement through dual-wavelength photoinitiation and photoinhibition. *ACS Macro Lett.* **8**, 899–904 (2019).
210. Rackson, C. M. et al. Object-space optimization of tomographic reconstructions for additive manufacturing. *Add. Manuf.* **48**, 102367 (2021).
211. Corbett, D. C. et al. Thermofluidic heat exchangers for actuation of transcription in artificial tissues. *Sci. Adv.* **6**, eabb9062 (2020).
212. Walker David, A., Hedrick James, L. & Mirkin Chad, A. Rapid, large-volume, thermally controlled 3D printing using a mobile liquid interface. *Science* **366**, 360–364 (2019).
213. Madrid-Sánchez, A. et al. Fabrication of large-scale scaffolds with microscale features using light sheet stereolithography. *Int. J. Bioprint.* **9**, 650 (2023).
214. Geng, Q., Wang, D., Chen, P. & Chen, S.-C. Ultrafast multi-focus 3-D nano-fabrication based on two-photon polymerization. *Nat. Commun.* **10**, 2179 (2019).
215. Maibohm, C. et al. Multi-beam two-photon polymerization for fast large area 3D periodic structure fabrication for bioapplications. *Sci. Rep.* **10**, 8740 (2020).
216. Oran, D. et al. 3D nanofabrication by volumetric deposition and controlled shrinkage of patterned scaffolds. *Science* **362**, 1281–1285 (2018).
217. Gong, J. et al. Complexation-induced resolution enhancement of 3D-printed hydrogel constructs. *Nat. Commun.* **11**, 1267 (2020).
218. Wang, M., Li, W., Garciamendez-Mijares, C. E. & Zhang, Y. S. Engineering (bio)materials through shrinkage and expansion. *Adv. Healthc. Mater.* **21**, 2100380 (2021).
219. Chung Li, C., Toombs, J. & Taylor, H. in *SCF '20: Proceedings of the 5th Annual ACM Symposium on Computational Fabrication 1–7* (ACM, 2020).
220. You, S., Wang, P., Schimelman, J., Hwang, H. H. & Chen, S. High-fidelity 3D printing using flashing photopolymerization. *Add. Manuf.* **30**, 100834 (2019).
221. Guan, J. et al. Compensating the cell-induced light scattering effect in light-based bioprinting using deep learning. *Bioprinting* **14**, 015011 (2021).
222. You, S. et al. Mitigating scattering effects in light-based three-dimensional printing using machine learning. *J. Manuf. Sci. Eng.* **142**, 081002 (2020).
223. Hsiao, K. et al. Single-digit-micrometer-resolution continuous liquid interface production. *Sci. Eng.* **8**, eabq2846 (2022).
224. FDA. *U.S. Food and Drug Administration Discussion Paper: 3D Printing Medical Devices at the Point of Care* (FDA, 2021).
225. Tahayeri, A. et al. 3D printed versus conventionally cured provisional crown and bridge dental materials. *Dent. Mater.* **34**, 192–200 (2018).
226. Liaw, C.-Y. & Guvendiren, M. Current and emerging applications of 3D printing in medicine. *Bioprinting* **9**, 024102 (2017).
227. Shen, E. M. & McCloskey, K. E. Affordable, high-resolution bioprinting with embedded concentration gradients. *Bioprinting* **21**, e00113 (2021).
228. Malda, J. et al. 25th Anniversary article: engineering hydrogels for biofabrication. *Adv. Mater.* **25**, 5011–5028 (2013).
229. Noor, N. et al. 3D printing of personalized thick and perfusable cardiac patches and hearts. *Adv. Sci.* **6**, 1900344 (2019).
230. Mouser, V. H. M. et al. Yield stress determines bioprintability of hydrogels based on gelatin-methacryloyl and gellan gum for cartilage bioprinting. *Bioprinting* **8**, 035003 (2016).
231. Sharaf, A. et al. Two-photon polymerization of 2.5 D and 3D microstructures fostering a ramified resting phenotype in primary microglia. *Front. Bioeng. Biotechnol.* **10**, 926642 (2022).
232. Arcuate, K., Mann, B. K. & Wicker, R. B. Stereolithography of three-dimensional bioactive poly(ethylene glycol) constructs with encapsulated cells. *Ann. Biomed. Eng.* **34**, 1429–1441 (2006).
233. Arcuate, K., Mann, B. K. & Wicker, R. B. Fabrication of off-the-shelf multilumen poly(ethylene glycol) nerve guidance conduits using stereolithography. *Tissue Eng.* **C17**, 27–38 (2011).
234. Rakin, R. H. et al. Tunable metacrylated hyaluronic acid-based hybrid bioinks for stereolithography 3D bioprinting. *Bioprinting* **13**, 044109 (2021).

### Acknowledgements

R.L. acknowledges funding from the European Research Council and from the FET-OPEN scheme under the European Union's Horizon 2020 research and innovation programme (grant agreement Nos. 949806 and 964497) and from the Netherlands Organization for Scientific Research (024.004.013 and NWA.1228.192.105). B.E.K. and K.S.A. acknowledge funding from the NIH (R01DE16523 and R01DK120921). J.S. acknowledges funding support from the NIH (F31NS125986). S.C. acknowledges funding from the NIH (R01CA253615, R33HD090662 and R21ES034455) and the National Science Foundation (1907434 and 2135720). M.Z.-W. acknowledges funding from Innosuisse (55019.1 IP-ENG), Y.S.Z. acknowledges funding from the NIH (R21EB025270, R01EB028143, R01HL165176 and R01HL166522), the National Science Foundation (1936105) and the Brigham Research Institute.

### Author contributions

Introduction (R.L., O.D. and Y.S.Z.); Experimentation (R.L., O.D., C.E.G.-M., B.E.K., K.S.A. and Y.S.Z.); Results (R.L., O.D. and Y.S.Z.); Applications (R.R., M.Z.-W. and Y.S.Z.); Reproducibility

and data deposition (R.L., O.D., C.E.G.-M. and Y.S.Z.); Limitations and optimizations (Y.S.Z. and R.L.); Outlook (J.S., S.C. and Y.S.Z.); Overview of the Primer (R.L. and Y.S.Z.); Reviewing and editing (all authors).

## Competing interests

Y.S.Z. consults for Allevi by 3D Systems and sits on the scientific advisory board and holds options of Xellar, both of which, however, did not participate in or bias the work. R.L. is a scientific advisor for Readily3D SA, which did not participate in or bias the work. The other authors declare no competing interests.

## Additional information

**Supplementary information** The online version contains supplementary material available at <https://doi.org/10.1038/s43586-023-00231-0>.

**Peer review information** *Nature Reviews Methods Primers* thanks Yan Han Huang, Liliang Ouyang and Wai Yee Yeong for their contribution to the peer review of this work.

**Publisher's note** Springer Nature remains neutral with regard to jurisdictional claims in published maps and institutional affiliations.

Springer Nature or its licensor (e.g. a society or other partner) holds exclusive rights to this article under a publishing agreement with the author(s) or other rightsholder(s); author self-archiving of the accepted manuscript version of this article is solely governed by the terms of such publishing agreement and applicable law.

## Related links

**3D Printing Database:** <http://cect.umd.edu/3d-printing-database>

**GitHub:** <http://github.com>

**Mendeley Data:** <http://data.mendeley.com>

**OpenExposer:** <https://hackaday.io/project/1129-openexposer>

**Zenodo:** <http://zenodo.org>

© Springer Nature Limited 2023